

Network Topology Inference from Smooth Signals Under Partial Observability*

Chuansen Peng, Hanning Tang, Zhiguo Wang, Xiaojing Shen

School of Mathematics, Sichuan University, Chengdu, Sichuan, 610064, China

Abstract

Inferring network topology from smooth signals is a significant problem in data science and engineering. A common challenge in real-world scenarios is the availability of only partially observed nodes. While some studies have considered hidden nodes and proposed various optimization frameworks, existing methods often lack the practical efficiency needed for large-scale networks or fail to provide theoretical convergence guarantees. In this paper, we address the problem of inferring network topologies from smooth signals with partially observed nodes. We propose a first-order algorithmic framework that includes two variants: one based on column sparsity regularization and the other on a low-rank constraint. We establish theoretical convergence guarantees and demonstrate the linear convergence rate of our algorithms. Extensive experiments on both synthetic and real-world data show that our results align with theoretical predictions, exhibiting not only linear convergence but also superior speed compared to existing methods. To the best of our knowledge, this is the first work to propose a first-order algorithmic framework for inferring network structures from smooth signals under partial observability, offering both guaranteed linear convergence and practical effectiveness for large-scale networks.

Key words: Graph learning; partial observability; network topology inference.

1 Introduction

Network topology inference from smooth signals has emerged as a pivotal area of research in the fields of machine learning and data science [1], [2], [3], [4]. The ability to infer the underlying graph structure from observed signals has profound implications for a wide array of applications [5], [6], ranging from social network analysis to sensor network localization [7]. This task is particularly challenging due to the inherent complexity of graph structures and the variability of signals.

The primary goal of network topology inference is to uncover the topology that best explains the observed data, often characterized by the smoothness of signals on the graph. This notion of smoothness is typically quantified by the graph Laplacian, which encodes the connectivity and edge weights of the graph. The objective is to learn a graph that minimizes the total variation of the sig-

nals, subject to constraints that reflect prior knowledge or desirable properties of the graph [8], [9].

Recent advancements in network topology inference have focused on developing efficient and robust algorithms that can handle large-scale datasets and accommodate various types of signals [10], [11], [12], [13], [14]. These methods often leverage optimization techniques [15], [16], [17], [18], spectral graph theory [19], and statistical inference [20], [21], [22], [23], [24] to iteratively refine the graph structure based on the observed data. The integration of these diverse mathematical tools has propelled the field forward, enabling the analysis of increasingly complex and high-dimensional datasets [25], [26], [27].

Despite notable advancements, several challenges persist in graph learning from smooth signals. A primary concern is the delicate balance between fidelity to observed data and the structural complexity of the inferred graph [28], [29]. Additionally, the presence of noise and the non-uniqueness of solutions pose significant barriers to obtaining accurate and reliable graph estimates [30], [31]. Moreover, the scalability of graph learning algorithms to massive datasets [32], [33] and the integration of dynamic or multi-modal signals demand sustained re-

* This paper was not presented at any IFAC meeting. Corresponding author Hanning Tang.

Email addresses: pengchuansen@stu.scu.edu.cn (Chuansen Peng), than.ning0@outlook.com (Hanning Tang), wangzhiguo@scu.edu.cn (Zhiguo Wang), shenxj@scu.edu.cn (Xiaojing Shen).

search efforts.

Specifically, the standard network-inference approach in existing works often assumes observations from all nodes of the graph are available. However, in certain environments, only observations from a subset of nodes are accessible, with the rest being unobserved or hidden. The existence of hidden nodes introduces a relevant and challenging problem, as closely related signal values from two observed nodes may be influenced not only by each other but also by a third latent node connected to both [34]. Furthermore, the absence of observations from hidden nodes complicates the network inference problem, rendering it more challenging and ill-posed. Network-inference studies that have addressed the issue of partial observability include examples in the context of Gaussian graphical model selection [35], [36] or nonlinear regression [37].

A commonly adopted strategy for solving network topology inference from smooth signals under partial observability involves formulating an optimization problem and then employing a CVX solver to compute solutions [34], [38]. In practice, we observe that CVX for solving graph learning with hidden variables tends to converge slowly for large-scaled networks. Consequently, there is an urgent imperative to devise algorithms that exhibit rapid convergence, thereby enhancing their applicability and efficiency in real-world scenarios. This recognition underscores the need for methodological innovation in graph learning, aiming to alleviate the computational burden and enable the effective analysis of large-scale graph structures.

In this article, based on the prior work and progress of [34], we introduce a first-order optimization framework for inferring network topology from smooth signals under partial observability and provide a rigorous convergence analysis of the algorithms. We summarize our principal contributions as follows:

- 1) In response to the practical network topology inference problem from smooth signals under partial observability in large-scale networks, we show that the problem can be reformulated as a optimization problem of separable objective functions with multiple blocks and linear equality constraints. Based on this, we propose a first-order algorithmic framework for graph learning from smooth signals under partial observability (GLOPSS). In particular, based on different regularization conditions, we present two variants of our algorithm: one is based on column sparsity regularization (GLOPSS-CS), and the other is underpinned by a low-rank constraint (GLOPSS-LR).
- 2) Building upon the convergence analysis work in [16], [39], we prove the linear convergence rate of GLOPSS. Furthermore, based on the structure of the optimization problem of GLOPSS, we establish a lower bound on the decrease in the norm of the

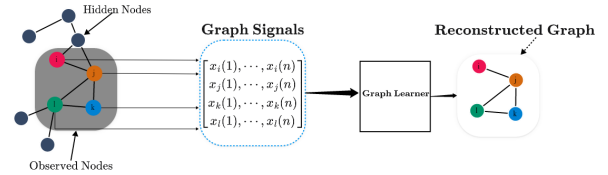


Fig. 1. Illustration of the network topology inference problem considered in this work (figure inspired by [40]).

difference between successive iterations and the optimal solution, and then proving that as long as the step sizes are bounded by the reciprocal of the largest singular value of the coefficient matrices, GLOPSS can linearly converge to the optimal solution of the target problem from any initial point. To the best of our knowledge, GLOPSS is the first provably linearly convergent first-order method for network topology inference from smooth signals under partial observability.

- 3) We provide extensive experiments on both synthetic and real-world data showing that GLOPSS aligns with theoretical predictions, exhibiting not only linear convergence but also superior speed compared to the state-of-the-art methods. The experimental data encompasses scenarios with different network sizes, number of latent nodes, noise power of the measurement. Both GLOPSS-CS and GLOPSS-LR exhibit higher accuracy and robustness, especially in the presence of noise and hidden nodes.

These contributions not only advance the theoretical foundations of graph learning but also offer a practical and effective algorithmic solution, underscoring the methodological innovation and potential impact of our approach.

The remainder of the paper is organized as follows. Section II introduces certain notations and fundamental concepts leveraged during the paper, and then formalizes the problem we aim to solve. Section III details the proposed algorithms (GLOPSS-CS and GLOPSS-LR). Section IV theoretically establishes the convergence guarantees of our algorithms and further demonstrate its linear convergence rate. The numerical evaluation of the proposed methods is presented in Section V, and Section VI provides some concluding remarks.

2 Problem Formulation

Prior to delineating the problem statement we aspire to resolve, we commence by elucidating certain notations and fundamental concepts.

2.1 Notations

For a positive integer m , let $[m] := \{1, 2, \dots, m\}$ denote the set of integers from 1 to m . The symbol $\mathbf{1}$ (resp. $\mathbf{0}$) represents the all-ones (resp. all-zeros) vector, with its dimensionality determined by the context.

Consider a graph $\mathcal{G} = (\mathcal{V}, \mathcal{E})$, where $\mathcal{V} = [m]$ denotes the set of nodes, and $\mathcal{E} \subseteq \mathcal{V} \times \mathcal{V}$ represents the set of edges. We assume that the graph does not contain self-loops, meaning $(i, i) \notin \mathcal{E}$ for all $i \in \mathcal{V}$. The graph is characterized by a symmetric and non-negative weight matrix $\mathbf{W} \in \mathbb{R}^{m \times m}$, where $W_{i,j} > 0$ if and only if $(i, j) \in \mathcal{E}$. A graph signal \mathbf{x} is typically represented as a column vector in \mathbb{R}^m , with its i -th component x_i indicating the signal value at vertex i . In numerous applications, the weight matrix \mathbf{W} is unknown, and our goal is to infer the latent graph structure \mathbf{W} from a collection of n graph signals $\mathbf{x}_1, \dots, \mathbf{x}_n \in \mathbb{R}^m$. The graph Laplacian matrix is defined as $\mathbf{L} := \text{Diag}(\mathbf{W}\mathbf{1}) - \mathbf{W}$. We denote the set of combinatorial Laplacians by \mathcal{L} , which is defined as:

$$\mathcal{L} := \{\mathbf{L} \in \mathbb{R}^{m \times m} \mid L_{ij} \leq 0 \text{ for } i \neq j; \mathbf{L} = \mathbf{L}^T; \mathbf{L}\mathbf{1} = \mathbf{0}; \mathbf{L} \succeq 0\}.$$

where $\mathbf{L} \succeq 0$ indicates that the Laplacian matrix is positive semi-definite (PSD).

For vectors \mathbf{a} and \mathbf{b} , we use the following notations:

- a_i denotes the i -th component of \mathbf{a} ,
- $\|\mathbf{a}\|_2$ represents the l_2 -norm of \mathbf{a} ,
- $\log(\mathbf{a})$ is element-wise logarithm of \mathbf{a} ,
- \mathbf{a}^2 denotes the element-wise square of \mathbf{a} ,
- $\sqrt{\mathbf{a}}$ represents the element-wise square root of \mathbf{a} ,
- $\text{Diag}(\mathbf{a})$ denotes a diagonal matrix with \mathbf{a} on its diagonal,
- \mathbf{a}/\mathbf{b} denotes element-wise division of \mathbf{a} by \mathbf{b} ,
- $\|\mathbf{a}\|_{\mathbf{A}} := (\mathbf{a}^T \mathbf{A} \mathbf{a})^{1/2}$ denotes the \mathbf{A} -norm of \mathbf{a} .

For matrices \mathbf{A} and \mathbf{B} , we use:

- A_{ij} for the (i, j) -th element of \mathbf{A} ,
- $\|\mathbf{A}\|_F$ for the Frobenius norm of \mathbf{A} ,
- $\|\mathbf{A}\|_{1,1}$ for the $L_{1,1}$ -norm of \mathbf{A} ,
- $\|\mathbf{A}\|_{2,1}$ for the $L_{2,1}$ -norm of \mathbf{A} ,
- $\|\mathbf{A}\|_2$ for spectral norm of \mathbf{A} ,
- $\|\mathbf{A}\|_*$ for the nuclear norm of \mathbf{A} ,
- $\|\mathbf{A}\|_{F,off}$ for the Frobenius norm excluding the element of the diagonal of \mathbf{A} ,
- $\text{diag}(\mathbf{A})$ for the vector of diagonal entries of \mathbf{A} ,
- $\mathbf{A} \odot \mathbf{B}$ for the Hadamard product of \mathbf{A} and \mathbf{B} ,
- $[\mathbf{A}; \mathbf{B}] := \begin{bmatrix} \mathbf{A} \\ \mathbf{B} \end{bmatrix}$ for the block column matrix formed by \mathbf{A} and \mathbf{B} .

For a vector \mathbf{a} , a set \mathcal{A} in the same space, and a positive semi-definite matrix \mathbf{A} , we use:

$$\mathbf{a} \rightarrow \mathbb{I}_{\mathcal{A}}(\mathbf{a}) := \begin{cases} 0, & \mathbf{a} \in \mathcal{A} \\ +\infty, & \mathbf{a} \notin \mathcal{A} \end{cases}$$

to denote the indicator function associated with \mathcal{A} and

$$\begin{aligned} \text{dist}(\mathbf{a}, \mathcal{A}) &:= \inf\{\|\mathbf{a} - \mathbf{b}\|_2 \mid \mathbf{b} \in \mathcal{A}\}, \\ \text{dist}_{\mathbf{A}}(\mathbf{a}, \mathcal{A}) &:= \inf\{\|\mathbf{a} - \mathbf{b}\|_{\mathbf{A}} \mid \mathbf{b} \in \mathcal{A}\} \end{aligned}$$

to denote the distance between \mathbf{a} and \mathcal{A} under the Euclidean norm and \mathbf{A} -norm, respectively.

For a proper extended real-valued function f , we define:

- $\text{dom}(f) := \{\mathbf{a} \mid f(\mathbf{a}) < +\infty\}$ as its domain,
- $\text{prox}_f(\mathbf{a}) := \arg \min_{\mathbf{b}} \{f(\mathbf{b}) + \frac{1}{2}\|\mathbf{b} - \mathbf{a}\|_2^2\}$ as the proximal mapping of f evaluated at $\mathbf{a} \in \text{dom}(f)$,
- $\partial f(\mathbf{a}) := \{\mathbf{c} \mid f(\mathbf{b}) \geq f(\mathbf{a}) + \mathbf{c}^T(\mathbf{b} - \mathbf{a}) \text{ for all } \mathbf{b}\}$ as the sub-differential of f at $\mathbf{a} \in \text{dom}(f)$.

Given a vectorizing mapping $\text{vec} : \mathbb{R}^{m \times m} \mapsto \mathbb{R}^{m^2}$, which vectorizes a matrix, (i.e., $\mathbf{w} = \text{vec}(\mathbf{W})$), the inverse mapping vec^{-1} satisfies $\mathbf{W} = \text{vec}^{-1}(\mathbf{w})$.

2.2 Graph Smoothness

To effectively perform graph learning, it is essential to understand the relationship between the graph structure and the graph signal. A common assumption is that the graph signal varies smoothly across the graph [11]. Intuitively, a signal is considered smooth if connected nodes with large edge weights have similar signal values. The smoothness of a signal \mathbf{x} on the graph \mathcal{G} is typically measured using the Laplacian quadratic form. This form involves the Laplacian matrix $\mathbf{L} = \text{Diag}(\mathbf{W}\mathbf{1}) - \mathbf{W}$ of \mathcal{G} and is defined as:

$$\mathbf{x}^T \mathbf{L} \mathbf{x} = \frac{1}{2} \sum_{i=1}^m \sum_{j=1}^m W_{ij} (x_i - x_j)^2,$$

quantifying the extent to which the signal \mathbf{x} fluctuates with respect to the notion of similarity encoded in the weights of \mathbf{W} . This measure will be referred to as the “local variation (LV)” of \mathbf{x} . To determine the average LV of n graph signals contained in the $m \times n$ matrix $\mathbf{X} = [\mathbf{x}_1, \dots, \mathbf{x}_n]$, compute:

$$\sum_{k=1}^n \mathbf{x}_k^T \mathbf{L} \mathbf{x}_k = \text{tr}(\hat{\mathbf{C}} \mathbf{L}), \quad (1)$$

where $\hat{\mathbf{C}} := \sum_{k=1}^n \mathbf{x}_k \mathbf{x}_k^T = \mathbf{X} \mathbf{X}^T$. Additionally, $\frac{1}{n} \hat{\mathbf{C}} = \frac{1}{n} \mathbf{X} \mathbf{X}^T$ provides the sample covariance estimate of \mathbf{X} .

2.3 Influence of Partial Observations in the Topology Inference Model

The current subsection is dedicated to formally delineating the topology-inference problem when observations are available only from a subset of nodes of the graph. We proffer a general formulation and underscore the impact of the concealed variables.

Let $\mathbf{X} = [\mathbf{x}_1, \dots, \mathbf{x}_n] \in \mathbb{R}^{m \times n}$ denote the compilation of n signals superimposed on the unbeknownst graph \mathcal{G} comprising m nodes. We then posit that observations are available solely from a subset of nodes $\mathcal{O} \subset \mathcal{V}$ with cardinality $o < m$ and the remaining $h = m - o$ nodes are unobserved, denoted by the subset $\mathcal{H} = \mathcal{V} \setminus \mathcal{O}$. For the sake of simplicity and without compromising generality, assume \mathcal{O} consists of the first o nodes of the graph. Thus, the observed signal matrix $\mathbf{X}_{\mathcal{O}} \in \mathbb{R}^{o \times n}$ comprises the first o rows of the matrix \mathbf{X} . We aim to discern the matrix $\hat{\mathbf{C}} \in \mathbb{R}^{m \times m}$ and the graph Laplacian $\mathbf{L} \in \mathbb{R}^{m \times m}$, which manifest the ensuing block configuration

$$\mathbf{X} = \begin{bmatrix} \mathbf{X}_{\mathcal{O}} \\ \mathbf{X}_{\mathcal{H}} \end{bmatrix}, \mathbf{L} = \begin{bmatrix} \mathbf{L}_{\mathcal{O}} & \mathbf{L}_{\mathcal{O}\mathcal{H}} \\ \mathbf{L}_{\mathcal{H}\mathcal{O}} & \mathbf{L}_{\mathcal{H}} \end{bmatrix}, \hat{\mathbf{C}} = \begin{bmatrix} \hat{\mathbf{C}}_{\mathcal{O}} & \hat{\mathbf{C}}_{\mathcal{O}\mathcal{H}} \\ \hat{\mathbf{C}}_{\mathcal{H}\mathcal{O}} & \hat{\mathbf{C}}_{\mathcal{H}} \end{bmatrix}. \quad (2)$$

The $o \times o$ matrix $\mathbf{L}_{\mathcal{O}}$ represents the Laplacian matrix of the observed nodes, whereas the residual blocks encapsulate the edges implicating concealed nodes. Analogously, $\frac{1}{n}\hat{\mathbf{C}}_{\mathcal{O}} = \frac{1}{n}\mathbf{X}_{\mathcal{O}}\mathbf{X}_{\mathcal{O}}^T$ denotes the sample covariance of the observed signals, while $1/n\hat{\mathbf{C}}_{\mathcal{O}\mathcal{H}}$ and $1/n\hat{\mathbf{C}}_{\mathcal{H}\mathcal{O}}$ correspond to the covariance involving hidden nodes. Given \mathcal{G} is undirected, both \mathbf{L} and $\hat{\mathbf{C}}$ are symmetric, thus, $\mathbf{L}_{\mathcal{H}\mathcal{O}} = \mathbf{L}_{\mathcal{O}\mathcal{H}}^T$ and $\hat{\mathbf{C}}_{\mathcal{H}\mathcal{O}} = \hat{\mathbf{C}}_{\mathcal{O}\mathcal{H}}^T$.

The graph learning/network topology inference problem under partial observations is formally introduced subsequently (also illustrated in Fig. 1).

Problem 1: Given a graph $\mathcal{G} = (\mathcal{V}, \mathcal{E})$ with m nodes and an unknown Laplacian matrix $\mathbf{L} \in \mathbb{R}^{m \times m}$, and the observations $\mathbf{X}_{\mathcal{O}} \in \mathbb{R}^{o \times n}$ corresponding to the values of n graph signals at the nodes in \mathcal{O} with $|\mathcal{O}| = o$, discern the underlying graph structure encoded $\mathbf{L}_{\mathcal{O}} \in \mathbb{R}^{o \times o}$ under the assumptions that:

(A1) The number of hidden nodes is much smaller than the number of observed nodes, i.e., $h \ll o$;

(A2) Graph signals $\mathbf{X} \in \mathbb{R}^{m \times n}$ varies smoothly across the graph.

Remark: Despite possessing observations from o nodes, the presence of $h = m - o$ hidden nodes complicates the inference of $\mathbf{L}_{\mathcal{O}}$, making the problem challenging, **(A1)**

simplifies the problem by limiting the number of concealed variables. Assumption **(A2)** ensures graph signals \mathbf{X} varies smoothly across the graph, with Equation (1) quantifying the smoothness of graph signals \mathbf{X} on the graph \mathcal{G} , which provides a relationship between the graph signals and the graph Laplacian matrix \mathbf{L} .

2.4 Problem Formulation of Topology Inference from Smooth Signals under Partial Observations

As previously discussed, to measure the smoothness of graph signals, we utilize the graph Laplacian and evaluate their LV as $\text{tr}(\mathbf{X}^T \mathbf{L} \mathbf{X})$. Here, we focus on $\hat{\mathbf{C}} = \mathbf{X} \mathbf{X}^T$. Due to the presence of hidden nodes, the entire covariance matrix is unobservable. To handle this, capitalizing on the block structure of $\hat{\mathbf{C}}$ and \mathbf{L} introduced in Equation (2), we can reformulate the LV of our dataset as

$$\text{tr}(\hat{\mathbf{C}} \mathbf{L}) = \text{tr}(\hat{\mathbf{C}}_{\mathcal{O}} \mathbf{L}_{\mathcal{O}}) + 2\text{tr}(\hat{\mathbf{C}}_{\mathcal{O}\mathcal{H}} \mathbf{L}_{\mathcal{O}\mathcal{H}}^T) + \text{tr}(\hat{\mathbf{C}}_{\mathcal{H}} \mathbf{L}_{\mathcal{H}}), \quad (3)$$

where only $\hat{\mathbf{C}}_{\mathcal{O}} = \mathbf{X}_{\mathcal{O}} \mathbf{X}_{\mathcal{O}}^T$ presumed to be known and the impact of hidden variables in the LV has been elucidated.

While the block-wise smoothness expression in (3) could be directly employed to approach the network topology inference as an optimization problem, the unknown submatrices necessitate estimation, making the problem non-convex if terms $\hat{\mathbf{C}}_{\mathcal{O}\mathcal{H}} \mathbf{L}_{\mathcal{O}\mathcal{H}}^T$ and $\hat{\mathbf{C}}_{\mathcal{H}} \mathbf{L}_{\mathcal{H}}$ are included. To circumvent this predicament, [34] introduce matrix $\mathbf{K} := \hat{\mathbf{C}}_{\mathcal{O}\mathcal{H}} \mathbf{L}_{\mathcal{O}\mathcal{H}}^T \in \mathbb{R}^{o \times o}$, leveraging its low-rank property due to $\text{rank}(\mathbf{K}) \leq h \ll o$. Similarly, matrix $\mathbf{R} := \hat{\mathbf{C}}_{\mathcal{H}} \mathbf{L}_{\mathcal{H}} \in \mathbb{R}^{h \times h}$ is a positive semi-definite matrices¹, ensuring $\text{tr}(\mathbf{R}) \geq 0$.

Thus, similar to [34], the network topology inference from smooth signals under partial observations is formulated as

$$\begin{aligned} \min_{\mathbf{L}_{\mathcal{O}}, \mathbf{K}, \mathbf{R}} \quad & \text{tr}(\hat{\mathbf{C}}_{\mathcal{O}} \mathbf{L}_{\mathcal{O}}) + 2\text{tr}(\mathbf{K}) + \text{tr}(\mathbf{R}) - \alpha \mathbf{1}^T \log(\text{diag}(\mathbf{L}_{\mathcal{O}})) \\ & + \beta \|\mathbf{L}_{\mathcal{O}}\|_{F, off}^2 + \gamma \|\mathbf{K}\|_* \\ \text{s.t.} \quad & \text{tr}(\hat{\mathbf{C}}_{\mathcal{O}} \mathbf{L}_{\mathcal{O}}) + 2\text{tr}(\mathbf{K}) + \text{tr}(\mathbf{R}) \geq 0, \\ & \text{tr}(\mathbf{R}) \geq 0, \\ & \mathbf{L}_{\mathcal{O}} \in \bar{\mathcal{L}}, \end{aligned} \quad (4)$$

where $\|\cdot\|_{F, off}$ denotes the Forbenius norm excluding the elements of the diagonal. This term, in conjunction with $\log(\text{diag}(\mathbf{L}_{\mathcal{O}}))$, controls the sparsity of $\mathbf{L}_{\mathcal{O}}$ and precludes the trivial solution of $\mathbf{L}_{\mathcal{O}} = \mathbf{0}$. The nuclear norm $\|\cdot\|_*$ encourages low-rank solutions for \mathbf{K} , and its incorporation ensure the convexity of (4), allowing for a globally

¹ Although in practical applications we might not know the exact value of h , the choice of h does not affect the formulation and solution of the subsequent optimization problem.

optimal solution. The parameters $\alpha, \beta, \gamma \geq 0$ balance the regularizers, with the first constraint ensuring non-negativity of LV and the second constraint encapsulating the positive semi-definiteness of \mathbf{R} . The final consideration is the form of $\bar{\mathcal{L}}$. It equates to the set of combinatorial Laplacians \mathcal{L} , but substituting the condition $\mathbf{L}\mathbf{1} = \mathbf{0}$ with $\mathbf{L}\mathbf{1} \geq \mathbf{0}$, i.e., $\bar{\mathcal{L}} := \{\mathbf{L} \in \mathbb{R}^{m \times m} \mid L_{ij} \leq 0, \text{ for } i \neq j; \mathbf{L} = \mathbf{L}^T; \mathbf{L}\mathbf{1} \geq \mathbf{0}; \mathbf{L} \succeq \mathbf{0}\}$, as $\mathbf{L}_{\mathcal{O}}$ is not a combinatorial Laplacian due to connections between observed and hidden nodes. This relaxation, while expanding the set of feasible solutions, complicates inference. To mitigate this, we shift to estimating $\tilde{\mathbf{L}}_{\mathcal{O}} := \text{Diag}(\mathbf{W}_{\mathcal{O}}\mathbf{1}) - \mathbf{W}_{\mathcal{O}}$, the Laplacian associated with the observed adjacency matrix $\mathbf{W}_{\mathcal{O}} \in \mathbb{R}^{o \times o}$ in which $\mathbf{W}_{\mathcal{O}}$ is the upper-left block of the partitioned matrix \mathbf{W} , i.e., similar to (2)

$$\mathbf{W} = \begin{bmatrix} \mathbf{W}_{\mathcal{O}} & \mathbf{W}_{\mathcal{O}\mathcal{H}} \\ \mathbf{W}_{\mathcal{H}\mathcal{O}} & \mathbf{W}_{\mathcal{H}} \end{bmatrix}.$$

Unlike $\mathbf{L}_{\mathcal{O}}$, $\tilde{\mathbf{L}}_{\mathcal{O}}$ is a valid combinatorial Laplacian, allowing reinstatement of the original Laplacian constraints.

Upon defining the $o \times o$ diagonal matrices $\mathbf{D}_{\mathcal{O}} := \text{Diag}(\mathbf{W}_{\mathcal{O}}\mathbf{1})$ and $\mathbf{D}_{\mathcal{O}\mathcal{H}} := \text{Diag}(\mathbf{W}_{\mathcal{O}\mathcal{H}}\mathbf{1})$, which enumerate the number of observed and concealed neighbors for the nodes in \mathcal{O} , the matrix $\mathbf{L}_{\mathcal{O}}$ is expressed as $\mathbf{L}_{\mathcal{O}} = \mathbf{D}_{\mathcal{O}} + \mathbf{D}_{\mathcal{O}\mathcal{H}} - \mathbf{W}_{\mathcal{O}} = \tilde{\mathbf{L}}_{\mathcal{O}} + \mathbf{D}_{\mathcal{O}\mathcal{H}}$. With this equivalence, the smoothness penalty in (3) is rewritten as

$$\begin{aligned} \text{tr}(\hat{\mathbf{C}}\mathbf{L}) &= \text{tr}(\hat{\mathbf{C}}_{\mathcal{O}}\tilde{\mathbf{L}}_{\mathcal{O}}) + \text{tr}(\hat{\mathbf{C}}_{\mathcal{O}}\mathbf{D}_{\mathcal{O}\mathcal{H}}) + 2\text{tr}(\mathbf{K}) + \text{tr}(\mathbf{R}) \\ &= \text{tr}(\hat{\mathbf{C}}_{\mathcal{O}}\tilde{\mathbf{L}}_{\mathcal{O}}) + 2\text{tr}(\tilde{\mathbf{K}}) + \text{tr}(\mathbf{R}), \end{aligned}$$

where $\tilde{\mathbf{K}} := \hat{\mathbf{C}}_{\mathcal{O}}\mathbf{D}_{\mathcal{O}\mathcal{H}}/2 + \mathbf{K}$. Owing to the entries of $\mathbf{D}_{\mathcal{O}\mathcal{H}}$ depend on the presence of edges between the observed and the hidden nodes, if the graph is sparse, the matrix $\mathbf{D}_{\mathcal{O}\mathcal{H}}$ will exhibit low-rank characteristics. Furthermore, since the sparsity pattern of the diagonal $\mathbf{D}_{\mathcal{O}\mathcal{H}}$ is contingent upon the matrix $\mathbf{W}_{\mathcal{O}\mathcal{H}} = -\mathbf{L}_{\mathcal{O}\mathcal{H}}$, it follows that the column sparsity pattern of $\hat{\mathbf{C}}_{\mathcal{O}}\mathbf{D}_{\mathcal{O}\mathcal{H}}$ aligns with that of \mathbf{K} , thereby implying that $\tilde{\mathbf{K}}$ also possesses low rank properties.

The optimization in (4) is then recast as

$$\begin{aligned} \min_{\tilde{\mathbf{L}}_{\mathcal{O}}, \mathbf{K}, r} \quad & \text{tr}(\hat{\mathbf{C}}_{\mathcal{O}}\tilde{\mathbf{L}}_{\mathcal{O}}) + 2\text{tr}(\tilde{\mathbf{K}}) + r - \alpha\mathbf{1}^T \log(\text{diag}(\tilde{\mathbf{L}}_{\mathcal{O}})) \\ & + \beta\|\tilde{\mathbf{L}}_{\mathcal{O}}\|_{F, off}^2 + \gamma_*\|\tilde{\mathbf{K}}\|_* + \gamma_{2,1}\|\tilde{\mathbf{K}}\|_{2,1} \\ \text{s.t.} \quad & \text{tr}(\hat{\mathbf{C}}_{\mathcal{O}}\tilde{\mathbf{L}}_{\mathcal{O}}) + 2\text{tr}(\tilde{\mathbf{K}}) + r \geq 0, \\ & r \geq 0, \\ & \tilde{\mathbf{L}}_{\mathcal{O}} \in \mathcal{L}, \end{aligned} \tag{5}$$

with $\bar{\mathcal{L}}$ in (4) has been substituted with \mathcal{L} in (5), which represents the set of all valid combinatorial Laplacian

matrices. Matrix \mathbf{R} is replaced by the non-negative variable r to simplify computation. Although we replaced \mathbf{K} with $\tilde{\mathbf{K}}$, it retains the same regularization properties. This formulation ensures a solution with the desired column sparsity and low-rank characteristics, with the flexibility to use either the nuclear norm or group LASSO penalty based on $\gamma_{2,1}$ and γ_* [34].

3 Proposed Optimization Framework

3.1 Problem Reformulation

In this context, let $\tilde{\mathbf{x}}_i := [(\mathbf{x}_1)_i, \dots, (\mathbf{x}_n)_i]^T$ denote the data vector associated with the i -th node and define $Z_{ij} := \|\tilde{\mathbf{x}}_i - \tilde{\mathbf{x}}_j\|_2^2$ as the squared pair-wise distance between the node vectors $\tilde{\mathbf{x}}_i, \tilde{\mathbf{x}}_j$. Subsequently, we derive the following expression, commonly recognized as the Dirichlet energy:

$$\begin{aligned} \sum_{k=1}^n \mathbf{x}_k^T \mathbf{L} \mathbf{x}_k &= \text{tr}(\hat{\mathbf{C}}\mathbf{L}) \\ &= \frac{1}{2} \sum_{i=1}^m \sum_{j=1}^m W_{ij} \|\tilde{\mathbf{x}}_i - \tilde{\mathbf{x}}_j\|_2^2 \\ &= \frac{1}{2} \|\mathbf{W} \odot \mathbf{Z}\|_{1,1}. \end{aligned}$$

Thus, equivalently, optimization problem (5) can be reformulated as²

$$\begin{aligned} \min_{\mathbf{W}_{\mathcal{O}} \in \mathbb{R}^{o \times o}, \tilde{\mathbf{K}}, r} \quad & \frac{1}{2} \|\mathbf{W}_{\mathcal{O}} \odot \mathbf{Z}_{\mathcal{O}}\|_{1,1} + 2\text{tr}(\tilde{\mathbf{K}}) + r + \beta\|\mathbf{W}_{\mathcal{O}}\|_F^2 \\ & - \alpha\mathbf{1}^T \log(\mathbf{W}_{\mathcal{O}}\mathbf{1}) + \gamma_*\|\tilde{\mathbf{K}}\|_* + \gamma_{2,1}\|\tilde{\mathbf{K}}\|_{2,1} \\ \text{s.t.} \quad & \mathbf{W}_{\mathcal{O}} \geq 0, \mathbf{W}_{\mathcal{O}} = \mathbf{W}_{\mathcal{O}}^T, \text{diag}(\mathbf{W}_{\mathcal{O}}) = \mathbf{0}, \\ & \frac{1}{2} \|\mathbf{W}_{\mathcal{O}} \odot \mathbf{Z}_{\mathcal{O}}\|_{1,1} + 2\text{tr}(\tilde{\mathbf{K}}) + r \geq 0, \\ & r \geq 0, \end{aligned} \tag{6}$$

where $\mathbf{Z}_{\mathcal{O}}$ is the upper-left block of the partitioned matrix \mathbf{Z} like (2).

Indeed, two distinct configurations of the objective function emerge based on the selection of regularization constants. By setting $\gamma_* = 0$, we encourage a solution that exhibits the desired column-sparsity property of the matrix $\tilde{\mathbf{K}}$. Conversely, setting $\gamma_{2,1} = 0$ leads to the promotion of a solution characterized by a reduced rank of $\tilde{\mathbf{K}}$ achieved through the imposition of nuclear norm regularization. This strategic manipulation of regularization

² In Problem 1, we need to find the graph Laplacian matrix $\mathbf{L}_{\mathcal{O}}$. Although in (6), we are finding the adjacency matrix $\mathbf{W}_{\mathcal{O}}$, since $\mathbf{L}_{\mathcal{O}} = \text{Diag}(\mathbf{W}_{\mathcal{O}}\mathbf{1}) - \mathbf{W}_{\mathcal{O}}$, if we can determine $\mathbf{W}_{\mathcal{O}}$, then $\mathbf{L}_{\mathcal{O}}$ can also be obtained.

parameters allows for the fine-tuning of the structural properties of $\tilde{\mathbf{K}}$ thereby enabling targeted optimization according to specific graph learning objectives.

Initially, we consider the scenario where $\gamma_* = 0$. Let \mathbf{w} (resp. \mathbf{z}) be the vector constructed by concatenating the entries above the main diagonal of $\mathbf{W}_{\mathcal{O}}$ (resp. $\mathbf{Z}_{\mathcal{O}}$) into a single column. Consequently, we have $\mathbf{w} \in \mathbb{R}^p$ and $\mathbf{z} \in \mathbb{R}^p$ with $p := o(o-1)/2$. Similarly, we define $\mathbf{k} := \text{vec}(\tilde{\mathbf{K}}) \in \mathbb{R}^{o^2}$. Thus, we can reformulate equation (6) as (with $\gamma_* = 0$)

$$\begin{aligned} \min_{\mathbf{w} \in \mathbb{R}^p, \mathbf{k} \in \mathbb{R}^{o^2}, r \in \mathbb{R}} & \frac{1}{2} \mathbf{z}^T \mathbf{w} + 2\mathbf{b}^T \mathbf{k} + r - \alpha \mathbf{1}^T \log(\mathbf{Bw}) \\ & + \beta \|\mathbf{w}\|_2^2 + \gamma_{2,1} h(\mathbf{k}) \\ \text{s.t.} & \mathbf{w} \geq 0, \\ & r \geq 0 \\ & \frac{1}{2} \mathbf{z}^T \mathbf{w} + 2\mathbf{b}^T \mathbf{k} + r \geq 0 \end{aligned} \quad (7)$$

where $h(\mathbf{k}) := \|\tilde{\mathbf{K}}\|_{2,1}$, and $\mathbf{B} \in \{0,1\}^{m \times p}$ and $\mathbf{b} \in \{0,1\}^{o^2}$ are defined such that:

$$\mathbf{Bw} = \mathbf{W1}, \quad (8)$$

$$\mathbf{b}^T \mathbf{k} = \text{tr}(\tilde{\mathbf{K}}). \quad (9)$$

Through the introduction of a relaxation variable $v \in \mathbb{R}_+$, and by setting $\frac{1}{2} \mathbf{z}^T \mathbf{w} + 2\mathbf{b}^T \mathbf{k} + r - v = 0$. Further refinement is obtained by introducing new variables $\mathbf{v} := [v_1; v_2]$ with $v_1 := r \in \mathbb{R}$, $v_2 = v \in \mathbb{R}$, new variables \mathbf{u} such that $\mathbf{Bw} = \mathbf{u}$ and denoting $\mathbf{a} := [1 \ -1]^T$, $\mathbf{d} := [1 \ 0]^T \in \mathbb{R}^2$. This leads to a subsequent reformulation of problem (7):

$$\begin{aligned} \min_{\mathbf{w}, \mathbf{u}, \mathbf{k}, \mathbf{v}} & f_1(\mathbf{w}) + f_2(\mathbf{u}) + f_3(\mathbf{k}) + f_4(\mathbf{v}) \\ \text{s.t.} & \frac{1}{2} \mathbf{z}^T \mathbf{w} + 2\mathbf{b}^T \mathbf{k} + \mathbf{a}^T \mathbf{v} = 0 \\ & \mathbf{Bw} = \mathbf{u}. \end{aligned} \quad (10)$$

where the functions are redefined as:

$$\begin{aligned} f_1(\mathbf{w}) &:= \frac{1}{2} \mathbf{z}^T \mathbf{w} + \beta \|\mathbf{w}\|_2^2 + \mathbb{I}_{\mathbb{R}_+^p}(\mathbf{w}), \\ f_2(\mathbf{u}) &:= -\alpha \mathbf{1}^T \log(\mathbf{u}), \\ f_3(\mathbf{k}) &:= 2\mathbf{b}^T \mathbf{k} + \gamma_{2,1} h(\mathbf{k}), \\ f_4(\mathbf{v}) &:= \mathbf{d}^T \mathbf{v} + \mathbb{I}_{\mathbb{R}_+}(\mathbf{v}), \end{aligned}$$

where $h(\mathbf{k}) = \|\tilde{\mathbf{K}}\|_{2,1}$.

Denoting $\mathbf{x} := [\mathbf{w}; \mathbf{u}; \mathbf{k}; \mathbf{v}]$, Problem 10 can be reformulated as

$$\begin{aligned} \min_{\mathbf{x}} & f(\mathbf{x}) = f_1(\mathbf{w}) + f_2(\mathbf{u}) + f_3(\mathbf{k}) + f_4(\mathbf{v}) \\ \text{s.t.} & \mathbf{Ax} = \mathbf{0}. \end{aligned} \quad (11)$$

where,

$$\begin{aligned} f_1(\mathbf{w}) &:= \frac{1}{2} \mathbf{z}^T \mathbf{w} + \beta \|\mathbf{w}\|_2^2 + \mathbb{I}_{\mathbb{R}_+^p}(\mathbf{w}), \\ f_2(\mathbf{u}) &:= -\alpha \mathbf{1}^T \log(\mathbf{u}), \\ f_3(\mathbf{k}) &:= 2\mathbf{b}^T \mathbf{k} + \gamma_{2,1} h(\mathbf{k}), \\ f_4(\mathbf{v}) &:= \mathbf{d}^T \mathbf{v} + \mathbb{I}_{\mathbb{R}_+}(\mathbf{v}) \\ \mathbf{A} &:= \begin{bmatrix} \frac{1}{2} \mathbf{z}^T & \mathbf{0} & 2\mathbf{b}^T & \mathbf{a}^T \\ \mathbf{B} & -\mathbf{I} & \mathbf{0} & \mathbf{0} \end{bmatrix}. \end{aligned}$$

Furthermore, we denote $\mathbf{M}_1 = [1/2\mathbf{z}^T; \mathbf{B}] \in \mathbb{R}^{(1+o) \times p}$, $\mathbf{M}_2 = [\mathbf{0}; -\mathbf{I}] \in \mathbb{R}^{(1+o) \times o}$, $\mathbf{M}_3 = [2\mathbf{b}^T; \mathbf{0}] \in \mathbb{R}^{(1+o) \times o^2}$ and $\mathbf{M}_4 = [\mathbf{a}^T; \mathbf{0}] \in \mathbb{R}^{(1+o) \times 2}$, so $\mathbf{A} = [\mathbf{M}_1^T; \mathbf{M}_2^T; \mathbf{M}_3^T; \mathbf{M}_4^T]^T$.

Remark: Although in practical applications we might not know the exact value of h , the choice of h does not affect the formulation and solution of our optimization problem. The reason is as follows: Originally, the matrices $\hat{\mathbf{C}}_{\mathcal{O}\mathcal{H}}$, $\mathbf{L}_{\mathcal{O}\mathcal{H}}$ and \mathbf{R} depend on h . However, by introducing a new matrix $\mathbf{K} := \hat{\mathbf{C}}_{\mathcal{O}\mathcal{H}} \mathbf{L}_{\mathcal{O}\mathcal{H}}^T \in \mathbb{R}^{o \times o}$, we make the matrix \mathbf{K} independent of h . Furthermore, although \mathbf{R} is a h -dimensional square matrix, our optimization objective only involves the trace of \mathbf{R} . To reduce computational and storage burdens, we substitute $\text{tr}(\mathbf{R})$ with a one-dimensional variable r . This substitution ensures that the choice of h does not affect the solution to our optimization problem (11).

3.2 Algorithmic Development

To begin, let $\lambda = [\lambda_1; \lambda_2] \in \mathbb{R}^{o+1}$ be the dual variable associated with the linear constraints $\mathbf{Ax} = \mathbf{0}$ in Problem (11), thus we can obtain the augmented Lagrangian function of the form

$$\mathcal{L}(\mathbf{x}; \lambda) = f(\mathbf{x}) - \lambda^T (\mathbf{Ax}) + \frac{\rho}{2} \|\mathbf{Ax}\|_2^2, \quad (12)$$

where $\rho \geq 0$ is a constant. The augmented dual function is given by

$$d(\lambda) = \min_{\mathbf{x}} f(\mathbf{x}) - \lambda^T \mathbf{Ax} + \frac{\rho}{2} \|\mathbf{Ax}\|_2^2 \quad (13)$$

In the i -th iteration (where $i \geq 0$), our GLOPSS-CS proceeds with the updates

$$\begin{aligned} \mathbf{w}^{i+1} &= \arg \min_{\mathbf{w} \in \mathbb{R}^p} \mathcal{L}(\mathbf{w}, \mathbf{k}^i, \mathbf{v}^i, \mathbf{u}^i; \lambda^i), \\ \mathbf{u}^{i+1} &= \arg \min_{\mathbf{u} \in \mathbb{R}^o} \mathcal{L}(\mathbf{w}^{i+1}, \mathbf{u}, \mathbf{k}^i, \mathbf{v}^i; \lambda^i), \\ \mathbf{k}^{i+1} &= \arg \min_{\mathbf{k} \in \mathbb{R}^{o^2}} \mathcal{L}(\mathbf{w}^{i+1}, \mathbf{u}^{i+1}, \mathbf{k}, \mathbf{v}^i; \lambda^i), \\ \mathbf{v}^{i+1} &= \arg \min_{\mathbf{v} \in \mathbb{R}^2} \mathcal{L}(\mathbf{w}^{i+1}, \mathbf{u}^{i+1}, \mathbf{k}^{i+1}, \mathbf{v}; \lambda^i), \\ \lambda^{i+1} &= \lambda^i - \rho \mathbf{A} \mathbf{x}^{i+1}. \end{aligned} \quad (14)$$

3.3 \mathbf{w} -Subproblem

We first provide the following proposition as preparation, with its proof deferred to the Appendix A.

Proposition 1 *If $f_1(\mathbf{w}) = \frac{1}{2}\mathbf{z}^T \mathbf{w} + \beta \|\mathbf{w}\|_2^2 + \mathbb{I}_{\mathbb{R}_+^p}(\mathbf{w})$, then for $\tau_1 > 0$, the closed-form proximal mapping of f_1 is given by*

$$\text{prox}_{\tau_1 f_1}(\mathbf{w}) = \max \left\{ \frac{\mathbf{w} - \frac{1}{2}\tau_1 \mathbf{z}}{2\tau_1\beta + 1}, \mathbf{0} \right\}.$$

Fixing \mathbf{k}^i , \mathbf{v}^i , \mathbf{u}^i and λ^i in the i -th iteration, the subproblem for \mathbf{w} is

$$\begin{aligned} \min_{\mathbf{w}} f_1(\mathbf{w}) - (\lambda^i)^T \mathbf{A}[\mathbf{w}; \mathbf{k}^i; \mathbf{v}^i; \mathbf{u}^i] + \frac{\rho}{2} \|\mathbf{A}[\mathbf{w}; \mathbf{k}^i; \mathbf{v}^i; \mathbf{u}^i]\|_2^2 \\ = \min_{\mathbf{w}} f_1(\mathbf{w}) + \frac{\rho}{2} \|\mathbf{A}[\mathbf{w}; \mathbf{k}^i; \mathbf{v}^i; \mathbf{u}^i] - \frac{\lambda^i}{\rho}\|_2^2 \end{aligned} \quad (15)$$

In view of Proposition 1, we linearize the quadratic term to perform one step of the proximal gradient iteration to update \mathbf{w}

$$\begin{aligned} \mathbf{w}^{i+1} &= \text{prox}_{\tau_1 f_1}(\mathbf{w}^i - \tau_1 \mathbf{e}_1^T \mathbf{A}^T (\mathbf{A} \mathbf{x}^i - \frac{\lambda^i}{\rho})) \\ &= \max\{\tilde{\mathbf{w}}^{i+1}, \mathbf{0}\}, \end{aligned} \quad (16)$$

where $\mathbf{e}_1 = [1; 0; 0; 0]^T \in \mathbb{R}^4$ and

$$\tilde{\mathbf{w}}^{i+1} = \frac{\mathbf{w}^i - \tau_1 \mathbf{B}^T (\mathbf{B} \mathbf{w}^i + \omega_2^i) + \omega_3^i - \frac{1}{4}\tau_1 \rho \mathbf{z} \mathbf{z}^T}{2\tau_1\beta + 1}.$$

Here, $\omega_1^i = 2\mathbf{b}^T \mathbf{k}^i + \mathbf{a}^T \mathbf{v}^i - \frac{\lambda_1^i}{\rho}$ is a constant, $\omega_2^i = -\mathbf{u}^i - \frac{\lambda_2^i}{\rho} \in \mathbb{R}^o$, and $\omega_3^i = -\frac{1}{2}\tau_1 \mathbf{z} - \frac{1}{2}\tau_1 \rho \omega_1^i \mathbf{z}$.

3.4 \mathbf{u} -Subproblem

We first provide the following lemma, adapted from [41], as preparation.

Lemma 2 *If $f_2(\mathbf{u}) = -\alpha \mathbf{1}^T \log(\mathbf{u})$, then for $\tau_2 > 0$, the closed-form proximal mapping of f_2 is given by*

$$\text{prox}_{\tau_2 f_2}(\mathbf{u}) = \frac{\mathbf{u} + \sqrt{\mathbf{u}^2 + 4\alpha\tau_2 \mathbf{1}}}{2},$$

where the square and the square root are both taken element-wise.

Fixing λ^i and the newly updated \mathbf{w}^{i+1} , the subproblem for \mathbf{u} is

$$\min_{\mathbf{u}} f_2(\mathbf{u}) + \frac{\rho}{2} \|\mathbf{A}[\mathbf{w}^{i+1}; \mathbf{k}^i; \mathbf{v}^i; \mathbf{u}] - \frac{\lambda^i}{\rho}\|_2^2. \quad (17)$$

Now, in view of Lemma 2, we perform similar proximal gradient iteration to update \mathbf{u}

$$\begin{aligned} \mathbf{u}^{i+1} &= \text{prox}_{\tau_2 f_2}(\mathbf{u}^i - \tau_2 \mathbf{e}_2^T \mathbf{A}^T (\mathbf{A} \mathbf{x}^i - \frac{\lambda^i}{\rho})) \\ &= \frac{\tilde{\mathbf{u}}^{i+1} + \sqrt{(\tilde{\mathbf{u}}^{i+1})^2 + 4\alpha\tau_2 \mathbf{1}}}{2}, \end{aligned} \quad (18)$$

where $\mathbf{e}_2 = [0; 1; 0; 0]^T \in \mathbb{R}^4$ and $\tilde{\mathbf{u}}^{i+1} = (1 - \tau_2 \rho) \mathbf{u}^i + \tau_2 \rho \mathbf{B} \mathbf{w}^{i+1} - \tau_2 \lambda_2^i / \rho$.

3.5 \mathbf{k} -Subproblem

Similarly, before we give the update of \mathbf{k} , we provide a lemma adapted from [42] as preparation.

Lemma 3 *Let $f : \mathbb{E} \rightarrow \mathbb{R}$ be a function given by $f(\mathbf{x}) := g(\|\mathbf{x}\|_2)$, where $g : \mathbb{R} \rightarrow (-\infty, +\infty]$ is a proper closed and convex function satisfying $\text{dom}(g) \subseteq [0, +\infty)$. Then*

$$\text{prox}_{\lambda f}(\mathbf{x}) = \begin{cases} \text{prox}_{\lambda g}(\|\mathbf{x}\|_2) \frac{\mathbf{x}}{\|\mathbf{x}\|_2}, & \mathbf{x} \neq \mathbf{0}, \\ \{\mathbf{u} \in \mathbb{E} : \|\mathbf{u}\|_2 = \text{prox}_{\lambda g}(\mathbf{0})\}, & \mathbf{x} = \mathbf{0}. \end{cases}$$

Combining Lemma 3, we can immediately have the following proposition, showing simple closed forms of the proximal mapping of f_3 , with its proof deferred to the Appendix B:

Proposition 4 *If $f_3(\mathbf{k}) = 2\mathbf{b}^T \mathbf{k} + \gamma_{2,1} h(\mathbf{k})$, then for $\tau_3 > 0$, the closed-form proximal mapping of f_3 is given by*

$$\text{prox}_{\tau_3 f_3}(\mathbf{k}) = \left[1 - \frac{\tau_3 \gamma_{2,1}}{\|\mathbf{k} - 2\tau_3 \mathbf{b}\|_2} \right]_+ (\mathbf{k} - 2\tau_3 \mathbf{b}),$$

if $\|\mathbf{k}\|_2 \neq 0$, else 0.

Fixing \mathbf{w}^{i+1} , \mathbf{u}^{i+1} , \mathbf{v}^i and λ^i , the subproblem for \mathbf{k} is

$$\begin{aligned} \mathbf{k}^{i+1} &= \arg \min_{\mathbf{k} \in \mathbb{R}^o} \mathcal{L}(\mathbf{w}^{i+1}, \mathbf{u}^{i+1}, \mathbf{k}, \mathbf{v}^i; \lambda^i) \\ &= \arg \min_{\mathbf{k}} f_3(\mathbf{k}) + \frac{\rho}{2} \|\mathbf{A}[\mathbf{w}^{i+1}; \mathbf{k}; \mathbf{v}^i; \mathbf{u}^{i+1}] - \frac{\lambda^i}{\rho}\|_2^2. \end{aligned} \quad (19)$$

In view of Proposition 4, we linearize the quadratic term to perform one step of the proximal gradient iteration to update \mathbf{k}

$$\begin{aligned} \mathbf{k}^{i+1} &= \text{prox}_{\tau_3 f_3}(\mathbf{k}^i - \tau_3 \mathbf{e}_3^T \mathbf{A}^T (\mathbf{A} \mathbf{x}^i - \frac{\lambda^i}{\rho})) \\ &= \left[1 - \frac{\tau_3 \gamma_{2,1}}{\|\tilde{\mathbf{k}}^{i+1}\|_2} \right]_+ \tilde{\mathbf{k}}^{i+1}, \end{aligned} \quad (20)$$

where $\mathbf{e}_3 = [0; 0; 1; 0]^T \in \mathbb{R}^4$ and

$$\begin{aligned}\tilde{\mathbf{k}}^{i+1} = & \mathbf{k}^i - \tau_3 2 \left(1 + \frac{1}{2} \rho \mathbf{z}^T \mathbf{w}^{i+1} \right. \\ & \left. + 2 \rho \mathbf{b}^T \mathbf{k}^i + \rho \mathbf{a}^T \mathbf{v}^i - \lambda_1^i \right) \mathbf{b}.\end{aligned}$$

3.6 v-Subproblem

Similarly, we provide a proposition as preparation, with its proof deferred to the Appendix C.

Proposition 5 *If $f_4(\mathbf{v}) = \mathbf{d}^T \mathbf{v} + \mathbb{I}_{\mathbb{R}_+}(\mathbf{v})$, then for $\tau_4 > 0$, the closed-form proximal mapping of f_4 is given by*

$$\text{prox}_{\tau_4 f_4}(\mathbf{v}) = \max\{\mathbf{v} - \tau \mathbf{d}\}.$$

Fixing the dual variable λ^i , newly updated \mathbf{w}^{i+1} , \mathbf{u}^{i+1} and \mathbf{k}^{i+1} , the subproblem for \mathbf{v} is

$$\begin{aligned}\mathbf{v}^{i+1} = & \arg \min_{\mathbf{v}} \mathcal{L}(\mathbf{w}^{i+1}, \mathbf{u}^{i+1}, \mathbf{k}^{i+1}, \mathbf{v}; \lambda^i) \\ = & \arg \min_{\mathbf{v}} f_4(\mathbf{v}) + \frac{\rho}{2} \|\mathbf{A}[\mathbf{w}^{i+1}; \mathbf{k}^{i+1}; \mathbf{v}; \mathbf{u}^{i+1}] - \frac{\lambda^i}{\rho}\|_2^2.\end{aligned}\quad (21)$$

In view of Proposition 5, we linearize the quadratic term to perform one step of the proximal gradient iteration to update \mathbf{v}

$$\mathbf{v}^{i+1} = \max\{\tilde{\mathbf{v}}^{i+1}, \mathbf{0}\}, \quad (22)$$

where

$$\tilde{\mathbf{v}}^{i+1} := \mathbf{v}^i - \tau_4 \mathbf{a}(s^{i+1} + \mathbf{a}^T \mathbf{v}) - \tau_4 \mathbf{d}$$

here, $s^{i+1} = \frac{1}{2} \mathbf{z}^T \mathbf{w}^{i+1} + 2 \mathbf{b}^T \mathbf{k}^{i+1} - \frac{\lambda_1^i}{\rho} \in \mathbb{R}$ is a constant.

3.7 Dual Variables Update

Subsequently, the dual variables λ is updated as:

$$\lambda^{i+1} = \lambda^i - \rho \mathbf{A} \mathbf{x}^{i+1}, \quad (23)$$

where $\mathbf{x}^{i+1} = [\mathbf{w}^{i+1}; \mathbf{k}^{i+1}; \mathbf{v}^{i+1}; \mathbf{u}^{i+1}]$.

The overall description of our GLOPSS-CS is given in Algorithm 1.

3.8 Low Rank Regularization

We have discussed the column-sparsity pattern of $\tilde{\mathbf{K}}$ above, while setting $\gamma_* = 0$. And next, we consider the nuclear norm regularization of $\tilde{\mathbf{K}}$ to promote a solution

Algorithm 1 Graph Learning from Smooth Signals under Partial Observability with Column Sparsity Regularization (GLOPSS-CS)

Input: penalty parameters α , β , $\gamma_{2,1}$ and ρ , step sizes $\tau_1, \tau_2, \tau_3, \tau_4$, primal residual tolerance ϵ_p , dual residual tolerance ϵ_d ,

Output: \mathbf{w}^* , \mathbf{k}^* , \mathbf{v}^* and \mathbf{u}^*

```

1: while  $r_p > \epsilon_p$  or  $r_d > \epsilon_d$  do
2:   update  $\mathbf{w}$  according to (16)
3:   update  $\mathbf{u}$  according to (18)
4:   update  $\mathbf{k}$  according to (20)
5:   update  $\mathbf{v}$  according to (22)
6:   update  $\lambda$  according to (23)
7:   set primal residual  $r_p = \|\mathbf{Bw}^{i+1} - \mathbf{u}^{i+1}\|_2$ 
8:   set dual residual  $r_d = \|\rho_2 \mathbf{B}^T (\mathbf{u}^{i+1} - \mathbf{u}^i)\|_2$ 
9:    $i \leftarrow i + 1$ 
10:  end while
```

with low rank on $\tilde{\mathbf{K}}$. Similarly, the algorithm (GLOPSS-LR) is the same as before, except the \mathbf{k} -subproblem. When $\gamma_{2,1} = 0$, we have the following lemma adapted from [42].

Lemma 6 *For a matrix $\mathbf{Y} \in \mathbb{R}^{m \times n}$, consider:*

$$\min_{\mathbf{X} \in \mathbb{R}^{m \times n}} \nu \|\mathbf{X}\|_* + \frac{1}{2} \|\mathbf{X} - \mathbf{Y}\|_F^2.$$

The optimal solution is:

$$\mathbf{X} := S(\mathbf{Y}, \nu) = \mathbf{U} \text{Diag}(s(\sigma, \nu)) \mathbf{V}^T,$$

where the singular value decomposition of \mathbf{Y} is $\mathbf{Y} = \mathbf{U} \text{Diag} \mathbf{V}^T$, and the thresholding operator is $s(\mathbf{x}, \nu) := \bar{\mathbf{x}}$ with

$$\bar{x}_i := \begin{cases} x_i - \nu, & \text{if } x_i - \nu > 0 \\ 0, & \text{otherwise.} \end{cases}$$

Now, the \mathbf{k} -subproblem becomes

$$\begin{aligned}\mathbf{k}^{i+1} = & \arg \min_{\mathbf{k} \in \mathbb{R}^{o^2}} \mathcal{L}(\mathbf{w}^{i+1}, \mathbf{u}^{i+1}, \mathbf{k}, \mathbf{v}^i; \lambda_1^i, \lambda_2^i) \\ = & 2 \mathbf{b}^T \mathbf{k} + \gamma_* \|\tilde{\mathbf{K}}\|_* \\ & + \frac{\rho}{2} \left(\frac{1}{2} \mathbf{z}^T \mathbf{w}^{i+1} + 2 \mathbf{b}^T \mathbf{k} + \mathbf{a}^T \mathbf{v}^i - \frac{\lambda_1^i}{\rho} \right) \\ = & f_{31}(\mathbf{k}) + f_{32}(\mathbf{k}),\end{aligned}\quad (24)$$

where,

$$\begin{aligned}f_{31}(\mathbf{k}) := & 2 \mathbf{b}^T \mathbf{k} + \frac{\rho}{2} \left(\frac{1}{2} \mathbf{z}^T \mathbf{w}^{i+1} + 2 \mathbf{b}^T \mathbf{k} + \mathbf{a}^T \mathbf{v}^i - \frac{\lambda_1^i}{\rho} \right)^2, \\ f_{32}(\mathbf{k}) := & \gamma_* \|\tilde{\mathbf{K}}\|_*.\end{aligned}$$

In view of Lemma 6, we linearize the quadratic term in $f_{31}(\mathbf{k})$ to perform one step of the proximal gradient

iteration to update \mathbf{k}

$$\begin{aligned}\mathbf{k}^{i+1} &= \text{prox}_{\tau_3 f_{32}}(\mathbf{k}^i - \tau_3 2(1 + \frac{1}{2}\rho \mathbf{z}^T \mathbf{w}^{i+1} \\ &\quad + 2\rho \mathbf{b}^T \mathbf{k}^i + \rho \mathbf{a}^T \mathbf{v}^i - \lambda_1^i) \mathbf{b}) \\ &= \text{vec}(\mathbf{U}^i \text{Diag}(s(\sigma^i, \gamma_*))(\mathbf{V}^i)^T),\end{aligned}\quad (25)$$

where \mathbf{U}^i and \mathbf{V}^i are composed by the left and right singular vectors of $\text{vec}^{-1}(\tilde{\mathbf{k}}^{i+1})$, i.e., $\text{vec}^{-1}(\tilde{\mathbf{k}}^{i+1}) = \mathbf{U}^i \text{Diag}(\sigma^i)(\mathbf{V}^i)^T$. Here we have $\tilde{\mathbf{k}}^{i+1} = \mathbf{k}^i - \tau_3 2(1 + \frac{1}{2}\rho \mathbf{z}^T \mathbf{w}^{i+1} + 2\rho \mathbf{b}^T \mathbf{k}^i + \rho \mathbf{a}^T \mathbf{v}^i - \lambda_1^i) \mathbf{b}$. And $s(\sigma^i, \gamma_*)$ is the thresholding operator:

$$s(\sigma^i, \gamma_*) = \bar{\sigma}^i, \text{ with } \bar{\sigma}_t^i := \begin{cases} \sigma_t^i - \nu, & \text{if } x_i - \nu > 0 \\ 0, & \text{otherwise} \end{cases}$$

where $t \in \{1, 2, \dots, o\}$.

The overall description of our GLOPSS-LR is given in Algorithm 2.

Algorithm 2 Graph Learning from Smooth Signals under Partial Observability with Low-Rank Regularization (GLOPSS-LR)

Input: penalty parameters $\alpha, \beta, \gamma_*, \rho$, step sizes $\tau_1, \tau_2, \tau_3, \tau_4$, primal residual tolerance ϵ_p , dual residual tolerance ϵ_d ,
Output: $\mathbf{w}^*, \mathbf{k}^*, \mathbf{v}^*$ and \mathbf{u}^*

- 1: **while** $r_p > \epsilon_p$ or $r_d > \epsilon_d$ **do**
- 2: update \mathbf{w} according to (16)
- 3: update \mathbf{u} according to (18)
- 4: update \mathbf{k} according to (25)
- 5: update \mathbf{v} according to (22)
- 6: update λ according to (23)
- 7: set primal residual $r_p = \|\mathbf{Bw}^{i+1} - \mathbf{u}^{i+1}\|_2$
- 8: set dual residual $r_d = \|\rho_2 \mathbf{B}^T (\mathbf{u}^{i+1} - \mathbf{u}^i)\|_2$
- 9: $i \leftarrow i + 1$
- 10: **end while**

4 Convergence Analysis

Suppose that $\alpha, \beta, \gamma_{2,1}(\gamma_*) > 0$. As discussed above, Problem (11) has a unique globally optimal solution $(\mathbf{w}^*, \mathbf{u}^*, \mathbf{k}^*, \mathbf{v}^*)$. In this section, we establish the global iteration convergence of Algorithm 1 and 2 following the techniques in [39], [15].

Observe that (11) is a linearly constrained convex optimization problem with at least one optimal solution.

Thus, its KKT conditions, which are given by

$$\begin{aligned}\mathbf{0} &\in \partial f_1(\mathbf{w}) - \frac{1}{2}\mathbf{z}\lambda_1 - \mathbf{B}^T \lambda_2, \\ \mathbf{0} &\in \partial f_2(\mathbf{u}) + \lambda_2, \\ \mathbf{0} &\in \partial f_3(\mathbf{k}) - 2\mathbf{b}\lambda_1, \\ \mathbf{0} &\in \partial f_4(\mathbf{v}) - \mathbf{a}\lambda_1, \\ \mathbf{0} &= \frac{1}{2}\mathbf{z}^T \mathbf{w} + 2\mathbf{b}^T \mathbf{k} + \mathbf{a}^T \mathbf{v}, \\ \mathbf{0} &= \mathbf{Bw} - \mathbf{u},\end{aligned}\quad (26)$$

are both necessary and sufficient for optimality. Let \mathbb{Q}^* denote the set of KKT points of Problem (11), i.e., $[\mathbf{w}; \mathbf{u}; \mathbf{k}; \mathbf{v}; \lambda_1; \lambda_2] \in \mathbb{Q}^*$ if and only if $(\mathbf{w}, \mathbf{u}, \mathbf{k}, \mathbf{v}, \lambda_1, \lambda_2)$ satisfies (26). Since GLOPSS-CS and GLOPSS-LR performs both primal and dual updates to generate the iterations $\{[\mathbf{w}^i; \mathbf{u}^i; \mathbf{k}^i; \mathbf{v}^i; \lambda_1^i; \lambda_2^i]\}_{i \geq 0}$, it is natural to ask whether these iterations converge to a KKT point of Problem (11), and if so, at what rate. We shall address these questions in this section.

4.1 Linear Convergence

Our proposed GLOPSS algorithm aligns with the ADMM framework in [39]. Building upon their seminal work, we immediately establish that our GLOPSS-CS and GLOPSS-LR algorithms globally converge linearly to an optimal solution to Problem (11), with its proof deferred to the Appendix D.

Theorem 7 *The sequence of iterations $\{\mathbf{w}^i, \mathbf{u}^i, \mathbf{k}^i, \mathbf{v}^i; \lambda^i\}$ generated by the GLOPSS-CS and GLOPSS-LR algorithms converge linearly to some point $[\mathbf{w}^*; \mathbf{u}^*; \mathbf{k}^*; \mathbf{v}^*; \lambda^*] \in \mathbb{Q}^*$ for (11), provided the step sizes τ_1, τ_2, τ_3 and τ_4 are sufficiently small.*

Theorem 7 reveals that the iteration sequence generated by GLOPSS-LR and GLOPSS-CS converge to some point in \mathbb{Q}^* at the linear rate. To the best of our knowledge, Theorem 7 furnishes the convergence guarantee known to date for addressing the graph learning formulation (11).

Moreover, based on the structure of GLOPSS-CS and GLOPSS-LR, we have found a connection between the step sizes and the maximum singular value of the coefficient matrices of the linear constraints in (11). Therefore, in the next subsection, we provide an upper bound on the step size that still ensures linear convergence, to guide the selection of step sizes in practical graph learning.

4.2 Selection of Step Sizes

To guide the selection of step sizes, one natural idea is to establish a lower bound on the decrease in the norm of

the difference between successive iterations and the optimal solution [15]. This result is instrumental in proving the convergence properties of the algorithm and ensuring its efficacy in solving graph learning problem (11). And then, we can give an upper bound of the step sizes according to the lower bound. To advance our analysis, we commence by stating the following theorem, with its proof deferred to the Appendix E:

Theorem 8 Suppose that $(\mathbf{w}^*, \mathbf{u}^*, \mathbf{k}^*, \mathbf{v}^*)$ is the optimal solution of Problem (11) and λ^* are the corresponding optimal dual variables. If the step sizes adhere to $\tau_1 < \frac{1}{\sigma_{\max}^2(\mathbf{M}_1)}, \tau_2 < \frac{1}{\sigma_{\max}^2(\mathbf{M}_2)}, \tau_3 < \frac{1}{\sigma_{\max}^2(\mathbf{M}_3)}, \tau_4 < \frac{1}{\sigma_{\max}^2(\mathbf{M}_4)}$, then there exists

$$c = \min\left\{\frac{\rho}{\tau_1} - \rho\sigma_{\max}^2(\mathbf{M}_1), \frac{\rho}{\tau_2} - \rho\sigma_{\max}^2(\mathbf{M}_2), \frac{\rho}{\tau_3} - \rho\sigma_{\max}^2(\mathbf{M}_3), \frac{\rho}{\tau_4} - \rho\sigma_{\max}^2(\mathbf{M}_4), \frac{1}{\rho} - \mu\right\} > 0$$

such that the sequence $\{(\mathbf{w}^i, \mathbf{u}^i, \mathbf{k}^i, \mathbf{v}^i, \lambda^i)\}_{i=0}^\infty$ generated by Algorithm 1 and 2 satisfies

$$\|\mathbf{y}^i - \mathbf{y}^*\|_{\mathbf{M}}^2 - \|\mathbf{y}^{i+1} - \mathbf{y}^*\|_{\mathbf{M}}^2 \geq c\|\mathbf{y}^i - \mathbf{y}^{i+1}\|_{\mathbf{M}}^2,$$

where $\sigma_{\max}(\cdot)$ denotes the largest singular value, $\mathbf{y}^i = [\mathbf{w}^i; \mathbf{u}^i; \mathbf{k}^i; \mathbf{v}^i; \lambda^i]$, $\mathbf{y}^* = [\mathbf{w}^*; \mathbf{u}^*; \mathbf{k}^*; \mathbf{v}^*; \lambda^*]$, $\mathbf{M} = \text{Diag}[\frac{\rho}{\tau_1}\mathbf{I} - \rho\mathbf{M}_1^T\mathbf{M}_1; \frac{\rho}{\tau_2}\mathbf{I} - \rho\mathbf{M}_2^T\mathbf{M}_2; \frac{\rho}{\tau_3}\mathbf{I} - \rho\mathbf{M}_3^T\mathbf{M}_3; \frac{\rho}{\tau_4}\mathbf{I}; \frac{1}{\rho}\mathbf{I}]$, and $\|\mathbf{y}\|_{\mathbf{M}} = \sqrt{\mathbf{y}^T\mathbf{M}\mathbf{y}}$ for $\mathbf{y} \in \mathbb{R}^{o^2+2o+p+3}$. Here, $\mu = (\frac{1}{2} + \frac{\tau_4\sigma_{\max}^2(\mathbf{M}_4)}{2})/\rho$.

As Theorem 8 suggests, the largest singular values of $\mathbf{M}_1, \mathbf{M}_2, \mathbf{M}_3$ and \mathbf{M}_4 dictate the maximum allowable values of τ_1, τ_2, τ_3 and τ_4 that ensure the global convergence of Algorithm 1 and 2. To guide the selection of step sizes, we present the following proposition, with its proof deferred to the Appendix F:

Proposition 9 The largest singular values of $\mathbf{M}_1, \mathbf{M}_2, \mathbf{M}_3$ and \mathbf{M}_4 satisfy

- (1) $\|\mathbf{M}_1\|_2 \leq \frac{1}{2}\kappa o + \sqrt{2(o-1)}$;
- (2) $\|\mathbf{M}_2\|_2 = 1$;
- (3) $\|\mathbf{M}_3\|_2 = 2\sqrt{o}$;
- (4) $\|\mathbf{M}_4\| = 2$ where κ^2 is the maximum component of $\mathbf{z}\mathbf{z}^T$.

We first use the definition of the projection mapping to rewrite the KKT conditions (26) as

$$\begin{aligned} \mathbf{w} - P_{X_1}(\mathbf{w} - (\partial f_1(\mathbf{w}) - \mathbf{M}_1^T\lambda)) &= \mathbf{0}, \\ \mathbf{u} - P_{X_2}(\mathbf{u} - (\partial f_2(\mathbf{u}) - \mathbf{M}_2^T\lambda)) &= \mathbf{0}, \\ \mathbf{k} - P_{X_3}(\mathbf{k} - (\partial f_3(\mathbf{k}) - \mathbf{M}_3^T\lambda)) &= \mathbf{0}, \\ \mathbf{v} - P_{X_4}(\mathbf{v} - (\partial f_4(\mathbf{v}) - \mathbf{M}_4^T\lambda)) &= \mathbf{0}, \\ \mathbf{Ax} &= \mathbf{0} \end{aligned} \quad (27)$$

where, $P_C(x) := \arg \min_{y \in C} \|x - y\|_2$ denotes the projection operator and $\mathbf{X} = X_1 \times X_2 \times X_3 \times X_4$ denotes

the feasible set with $\mathbf{w} \in X_1$, $\mathbf{u} \in X_2$, $\mathbf{k} \in X_3$, and $\mathbf{v} \in X_4$. Next, we define the projection KKT mapping $\mathcal{E} : \mathbb{R}^{o^2+2o+p+3} \rightarrow \mathbb{R}^{o^2+2o+p+3}$, associated with Problem (11) as

$$\mathcal{E}(\mathbf{w}, \mathbf{u}, \mathbf{k}, \mathbf{v}, \lambda) := \begin{bmatrix} \mathbf{w} - P_{X_1}(\mathbf{w} - (\partial f_1(\mathbf{w}) - \mathbf{M}_1^T\lambda)) \\ \mathbf{u} - P_{X_2}(\mathbf{u} - (\partial f_2(\mathbf{u}) - \mathbf{M}_2^T\lambda)) \\ \mathbf{k} - P_{X_3}(\mathbf{k} - (\partial f_3(\mathbf{k}) - \mathbf{M}_3^T\lambda)) \\ \mathbf{v} - P_{X_4}(\mathbf{v} - (\partial f_4(\mathbf{v}) - \mathbf{M}_4^T\lambda)) \\ \mathbf{Ax} \end{bmatrix}. \quad (28)$$

It is well known that error bounds furnish a powerful tool for establishing convergence rates of various iterative methods; see, e.g., [16], [39], [43], [44]. In particular, the following result, which shows that the mapping $\mathcal{E}(\mathbf{y})$ possesses the so-called error bound property, is a direct consequence of [16]:

Lemma 10 The mapping $\mathcal{E}(\mathbf{y})$ is metrically subregular at any KKT point of Problem (11). Specifically, there exists a constant $\zeta > 0$ and a neighborhood $\mathcal{U} \subseteq \mathbb{R}^{\ell} (\ell = o^2 + 2o + p + 3)$ with $\mathcal{Q}^* \subseteq \mathcal{U}$ such that whenever $\mathbf{y} \in \mathcal{U}$, we have

$$\text{dist}(\mathbf{y}, \mathcal{Q}^*) \leq \zeta \text{dist}(\mathbf{0}, \mathcal{E}(\mathbf{y})).$$

To get the linear convergence of GLOPSS-CS and GLOPSS-LR, we need to establish relationship between $\|\mathbf{y}^{i+1} - \mathbf{y}^i\|_{\mathbf{M}}$ and $\text{dist}(\mathbf{0}, \mathcal{E}(\mathbf{y}^{i+1}))$, which is shown in the following lemma with its proof deferred to Appendix G:

Lemma 11 Let $\mathbf{y}^{i+1} = \{\mathbf{w}^i, \mathbf{u}^i, \mathbf{k}^i, \mathbf{v}^i, \lambda^i\}$ be the sequence generated by GLOPSS-LR or GLOPSS-CS. There exists $\eta > 0$ such that

$$\|\mathbf{y}^i - \mathbf{y}^{i+1}\|_{\mathbf{M}}^2 \geq \eta \text{dist}^2(\mathbf{0}, \mathcal{E}(\mathbf{y}^{i+1})).$$

Combining Lemma 11 and the inequality $\text{dist}(\mathbf{y}, \mathcal{Q}^*) \leq \zeta \text{dist}(\mathbf{0}, \mathcal{E}(\mathbf{y}))$ in Lemma 10, we have

$$\|\mathbf{y}^{i+1} - \mathbf{y}^i\|_{\mathbf{M}}^2 \geq \eta \text{dist}^2(\mathbf{0}, \mathcal{E}(\mathbf{y}^{i+1})) \geq \frac{\eta}{\zeta^2} \text{dist}^2(\mathbf{y}^{i+1}, \mathcal{Q}^*). \quad (29)$$

Select $\mathbf{y}^* \in \mathcal{Q}^*$ such that $\text{dist}_{\mathbf{M}}(\mathbf{y}^i, \mathcal{Q}^*) = \|\mathbf{y}^i - \mathbf{y}^*\|_{\mathbf{M}}$.

Then, we have

$$\begin{aligned}
& (1 + \frac{c\eta}{\zeta^2}) \text{dist}_{\mathbf{M}}^2(\mathbf{y}^{i+1}, \mathbb{Q}^*) \\
& \leq \|\mathbf{y}^{i+1} - \mathbf{y}^*\|_{\mathbf{M}}^2 + \frac{c\eta}{\zeta^2} \text{dist}_{\mathbf{M}}^2(\mathbf{y}^{i+1}, \mathbb{Q}^*) \\
& \leq \|\mathbf{y}^{i+1} - \mathbf{y}^*\|_{\mathbf{M}}^2 + c\|\mathbf{y}^{i+1} - \mathbf{y}^i\|_{\mathbf{M}}^2 \\
& \leq \|\mathbf{y}^i - \mathbf{y}^*\|_{\mathbf{M}}^2 \\
& = \text{dist}_{\mathbf{M}}^2(\mathbf{y}^i, \mathbb{Q}^*), \tag{30}
\end{aligned}$$

where the second and the third inequalities follow from (29) and Theorem 8. Now we draw the linear convergence of GLOPSS-CS and GLOPSS-LR in the following theorem.

Theorem 12 Suppose the step sizes adhere to $\tau_1 < \frac{1}{\sigma_{\max}^2(\mathbf{M}_1)}$, $\tau_2 < \frac{1}{\sigma_{\max}^2(\mathbf{M}_2)}$, $\tau_3 < \frac{1}{\sigma_{\max}^2(\mathbf{M}_3)}$, $\tau_4 < \frac{1}{\sigma_{\max}^2(\mathbf{M}_4)}$, let $\{\mathbf{w}^i, \mathbf{u}^i, \mathbf{k}^i, \mathbf{v}^i, \lambda^i\}$ be the sequence generated by Algorithm 1 or 2. Then, there exists $0 < \varrho < 1$ such that

$$\text{dist}_{\mathbf{M}}(\mathbf{y}^{i+1}, \mathbb{Q}^*) \leq \varrho \text{dist}_{\mathbf{M}}(\mathbf{y}^i, \mathbb{Q}^*).$$

Remark: Theorem 12 ensures the linear convergence of Algorithm 1 and 2 with an arbitrary initial point, provided that appropriate step sizes are chosen. In light of Proposition 9, we should select $\tau_1 < \frac{1}{(\frac{1}{2}\kappa\sigma + \sqrt{2(\sigma-1)})^2}$,

$\tau_2 < 1$, $\tau_3 < \frac{1}{4\sigma}$ and $\tau_4 < \frac{1}{2}$ when addressing the graph learning model. This convergence analysis not only validates the efficacy of our GLOPSS-CS and GLOPSS-LR algorithms but also provides practical guidelines for selecting step sizes, thereby enhancing its applicability in solving graph learning problems.

In conclusion, we have demonstrated that when applied to the graph learning formulation (11), the iterations generated by our proposed GLOPSS-CS and GLOPSS-LR algorithms converge to a KKT point of the formulation at a linear rate. To the best of our knowledge, our work represents the pioneering development of a first-order method tailored to the graph learning formulation encapsulated in (11), accompanied by a linear convergence guarantee. This result not only enhances the theoretical foundations of graph learning but also offers a practical and effective algorithmic solution, underscoring the methodological innovation and potential impact of our approach.

5 Numerical Experiments

This section presents numerical experiments to evaluate and compare the proposed algorithms. We assess their performance using synthetic data and real-world datasets, implemented in MATLAB. For comparison, because the classic ADMM framework only has two block, we may consider grouping the 4 blocks in (11)

into 2 blocks. Here, we group \mathbf{w} and \mathbf{v} as one block and \mathbf{u} and \mathbf{k} as another one³, therefore, the constraint in (11) can be rewritten as

$$\begin{pmatrix} \frac{1}{2}\mathbf{z}^T \mathbf{a}^T \\ \mathbf{B} \end{pmatrix} \begin{pmatrix} \mathbf{w} \\ \mathbf{v} \end{pmatrix} + \begin{pmatrix} 2\mathbf{b}^T & \mathbf{0} \\ \mathbf{0} & -\mathbf{I} \end{pmatrix} \begin{pmatrix} \mathbf{k} \\ \mathbf{u} \end{pmatrix} = \mathbf{0}. \tag{31}$$

For convenience in describing the experiment later, we will refer the variables grouping method discussed above as GraSS. Similar to GLOPSS, GraSS has two variants based on different regularization constraints, namely GraSS-CS and GraSS-LR. Based on the numerical experiments, we have discovered that GraSS-LR and GraSS-CS, with smaller maximum singular values of the coefficient matrices among all possible variable partitions, are expected to perform faster than other partitioning methods. Given the close performance between GraSS-CS and GraSS-LR, we elect to compare only one of them (GraSS-LR) with GLOPSS-LR, which does not consider variable partitioning. We will focus on comparing the convergence performance of GLOPSS-LR and GraSS-LR. We will also show the runtime comparison of GLOPSS and Gsm-GL (Gsm-LR) proposed by [34], who use CVX as a solver. After that, we will also compare GLOPSS with GL-SigRep, as described in [45], highlighting the advantage of considering hidden nodes in the recovery process. The parameters α , β and $\gamma_{2,1}$ (or γ_*) in Problem (11) are best-tuned to maximize the quality of the learned graphs based on the F-measure. Additionally, parameters ρ and step size τ in GraSS-LR and GLOPSS-LR with GLOPSS-CS are also finely-tuned to achieve optimal convergence rates.

5.1 Graph Learning Experiments

1) *Experimental Setup:* Following [45], we generate smooth signals \mathbf{X} , using the eigen-decomposition of the graph Laplacian $\mathbf{L} = \mathbf{V}\Lambda\mathbf{V}^T$, where $\mathbf{L} = \text{Diag}(\mathbf{W}\mathbf{1}) - \mathbf{W}$. The signals matrix $\mathbf{X} = \mathbf{V}\mathbf{Z} + \epsilon$ is composed of $\mathbf{Z} \in \mathbb{R}^{m \times n}$, drawn from a multivariate Gaussian distribution $\mathbf{Z} \sim \mathcal{N}(\mathbf{0}, \Lambda^\dagger)$, where Λ^\dagger is the pseudo-inverse of matrix Λ , and Gaussian noise $\epsilon \sim \mathcal{N}(\mathbf{0}, \sigma\mathbf{I})$ with noise level σ . We evaluate recovery performance using weighted graphs and employ the F_{score} :

$$F_{\text{score}} = 2 \cdot \frac{\text{precision} \cdot \text{recall}}{\text{precision} + \text{recall}},$$

³ Theoretically, one can group the 4 block variables into two blocks with any combination. However, the numerical performance of different partitions of the variables can vary significantly, as the step sizes of the proximal gradient steps are linked to the largest singular values of the coefficient matrices. The partition in (27) allows larger step size for the first subproblem, thus, GraSS is faster than any other grouping variables methods except the no grouping one.

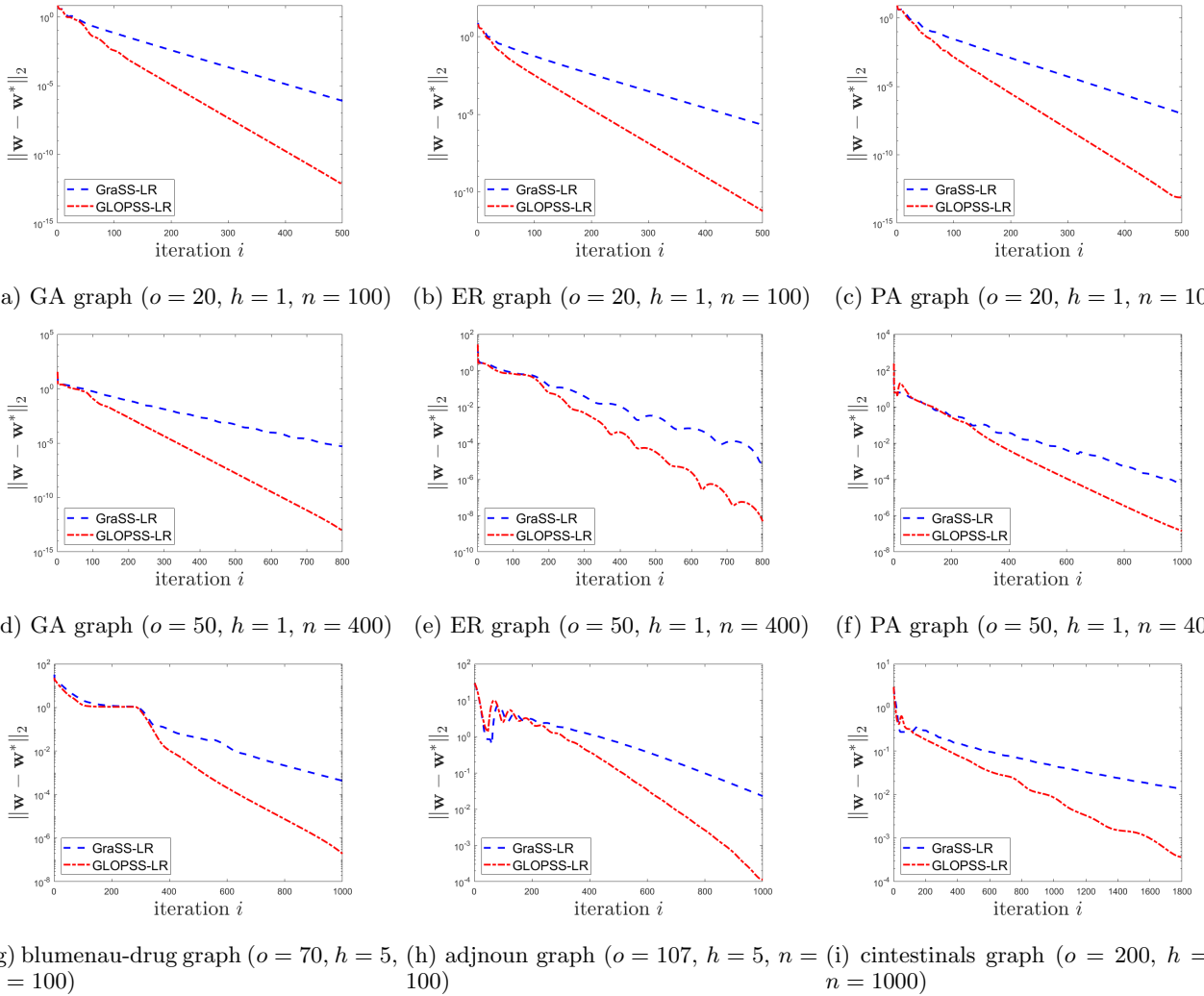


Fig. 2. Convergence performance of GLOPSS-LR for graph learning on synthetic graphs

where *precision* is the fraction of estimated edges that match the ground-truth edges and *recall* the fraction of actual edges correctly identified.

2) *Synthetic Graph*: We experiment with three types of synthetic graphs: the Gaussian (GA) graph, the Erdős-Rényi (ER) graph, the preferential attachment (PA) graph. In the Gaussian graph, nodes are randomly placed in a unit square, with edges added based on a radial basis function with a threshold of 0.75. For example, an edge is placed between node i and j if the weight determined by the radial basis function $\exp(-d(i,j)^2/2\theta^2)$, where $d(i,j)$ is the Euclidean distance between nodes i and j and $\theta = 0.5$ is the kernel width parameter, is at least 0.75. The ER graph connects nodes independently with probability 0.2, while the PA graph adds new nodes, connecting each to a previous node with probability proportional to previous node's degree. The edges in the Gaussian graph have weights given by the radial basis function, while those

in the ER and PA are set to 1. We use a noise level of $\sigma = 0.5$ for all graphs.

Given the $\mathcal{O}(m^2)$ per-iteration computational cost of the algorithms, with m being the dimension of graph signals, we measure their performance through the suboptimality gap $\|\mathbf{w}^i - \mathbf{w}^*\|_2$ for various m and n (number of graph signals). The average numerical performance of GLOPSS-LR for different graphs over 10 random testings is displayed and summarized in Fig. 2. As shown in Fig. 2, GLOPSS-LR converges noticeably more rapidly than GraSS-LR across all graph types. For instance, with the ER graph of $m = 21$, GraSS-LR requires approximately 350 iterations to achieve suboptimality gap $\|\mathbf{w} - \mathbf{w}^*\|$ below 10^{-5} , while GLOPSS-LR does so in about 150 iterations. This aligns with our theoretical findings, as GLOPSS-LR not only allows for larger step sizes but also enables subsequent variables to exploit the most recent updates of preceding variables during each iteration, thus converging more rapidly than methods

that consider variable partitioning.

3) *Real-World Graphs*: We also test the numerical performance of the algorithms on several real-world graphs from Netzschleuder ⁴: the Blumenau-drug network [46] with $m = 75$, the Adjnoun network [47] with $m = 112$ and the Cintestinalis network [48] with $m = 205$. The numerical results, shown in Fig. 2 indicate that GLOPSS-LR converges much faster than GraSS-LR in most cases. Even for the relatively larger Cintestinalis network, GLOPSS-LR can still achieve precision of 10^{-4} , more quickly than GraSS-LR.

5.2 Runtime Comparison

Next, we will show the runtime comparison of GLOPSS, GraSS and Gsm-GL (Gsm-LR) proposed by [34], who use CVX as a solver. We evaluate the CPU runtime of GLOPSS-CS and GLOPSS-LR algorithms by terminating it when the suboptimality gap $\|\mathbf{w}^i - \mathbf{w}^*\|_2$ falls below 10^{-6} . Given that Problem (11) is convex, we use the CVX package [49] with SDPT3 as the solver and set the precision to the highest available level. The runtime of Gsm-GL and Gsm-LR are provided as baselines for comparison.

Table 1. presents the average runtime across 10 independent trials under the same experiment settings as those used in Fig. 2. The results indicate that GLOPSS-LR and GLOPSS-CS generally require less runtime compared to GraSS-LR. Notably, for the medium-sized networks such as Adjnoun and Blumenau-drug networks, GLOPSS-LR and GLOPSS-CS show a significant reduction in runtime compared to both CVX and GraSS-LR. We do not provide runtime comparison for the largest Cintestinalis graph, as all the compared methods except GLOPSS-LR and GLOPSS-CS exhibit exceedingly slowly convergence. We can also find that GLOPSS-CS and GLOPSS-LR have the similar performance. The choice of two algorithms depends on the specific needs of the application, and there is no definitive answer as to which is superior or inferior.

5.3 Influence of Latent Nodes

Fig. 3 illustrates the variation in F_{score} as the number of hidden nodes h increases, for various recovery algorithms. Graphs are randomly generated using the model in [45], with hidden nodes chosen uniformly at random from the entire graph. The algorithms tested include: (i) GL-SigRep, as described in [45]; (ii) Gsm-GL and Gsm-LR, as described in [34]; (iii) GLOPSS-CS, as described in Algorithm 1, which employs column-sparsity promotion in $\tilde{\mathbf{K}}$ via group LASSO with $\gamma_* = 0$; and (iv) GLOPSS-LR, the low-rank regularized algorithm from Algorithm 2.

⁴ <https://networks.skewed.de/>

Comparing GL-SigRep with GLOPSS-LR allows us to assess the benefit of incorporating hidden variables into the model. Results from Fig. 3 show that, although all algorithms experience performance deteriorate as the number of hidden variables increases, GLOPSS-CS and GLOPSS-LR, which account for the presence of hidden variables, outperform the alternatives. Their performance decline is slower with increasing h , demonstrating the importance of accounting for hidden variables. The observed overall performance decline is expected as more hidden variables renders the topology inference problem more challenging and ill-posed. Comparing GLOPSS-CS with GLOPSS-LR, their performances are similar, reflecting the sparsity of the generated graphs. We also found that the performance of Gsm-LR (resp. Gsm-GL) and GLOPSS-LR (resp. GLOPSS-CS) is almost identical, which is as expected since the optimal solutions of the two algorithms are the same. Our proposed GLOPSS algorithm, which converges linearly, simply offers faster computation, enabling quicker convergence to this single optimal solution.

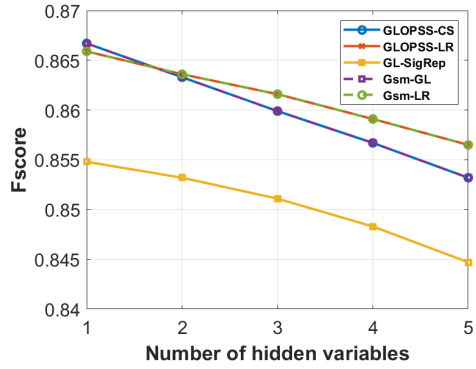


Fig. 3. Median F_{score} for GLOPSS-GL and GLOPSS-LR based on smooth siganls with $m = 25$ and $n = 100$ while the number of hidden variables h varing from 1 to 5 when using Gaussian graphs.

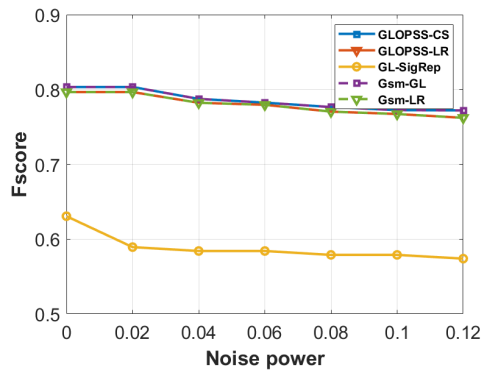


Fig. 4. F_{score} for GLOPSS-GL and GLOPSS-LR based on smooth siganls with $m = 25$ and $n = 100$ while the noise level present in the observations \mathbf{X} when using ER graphs with link probability $p = 0.2$.

Table 1

Runtime of Algorithms for Graph Learning from Smooth Signals Under Partial Observability

	o	Gsm-GL	Gsm-LR	GraSS-LR	GLOPSS-CS	GLOPSS-LR
Gaussian	20	2.1	1.9	0.0023	0.0019	0.00185
	50	15.5	14.7	0.1198	0.0894	0.0803
ER	20	4.3	4.8	0.00828	0.0064	0.007
	50	13.8	13.1	0.1058	0.0613	0.0605
PA	20	2.3	2.6	0.0131	0.0014	0.0046
	50	13.2	12.84	0.1159	0.0519	0.05
(a) Runtime (in seconds) on synthetic graphs						
	o	Gsm-GL	Gsm-LR	GraSS-LR	GLOPSS-CS	GLOPSS-LR
blumenau	70	16.84	15.9	0.248	0.083	0.098
adjnoun	107	474.8	443.6	1.043	0.72	0.665
(b) Runtime (in seconds) on real-world graphs						

5.4 Robustness

The experiments assumes that the observations $\mathbf{X}_\mathcal{O}$ correspond to the ground-truth signals corrupted by additive white Gaussian noise. For experiments with additive white Gaussian noise, we evaluate the link-identification performance by measuring the F_{score} of GL-SigRep, GLOPSS-CS and GLOPSS-LR as noise power increases. Using ER graphs with edge probability $p = 0.2$ and one hidden variables ($h = 1$), results in Fig. 4 reveal that the performance declines with increasing noise level. Despite not being specifically designed to handle noisy observations, the proposed algorithms exhibit a slower rate of F_{score} degradation relative to the increase in noise power, demonstrating their robustness. Moreover, our algorithm consistently outperform GL-SigRep, highlighting the advantage of considering hidden nodes in the recovery process.

6 Conclusion

In this article, we present a highly efficient and versatile optimization approach for network topology inference from smooth signals under partial observability. We have demonstrated that our method achieves linear convergence to the optimal solution by showing that the KKT points of the formulation possess an error bound property. Extensive numerical experiments, conducted on both synthetic and real-world datasets, confirm that our algorithms outperform existing state-of-the-art methods in terms of both convergence speed and computational efficiency. Future research could explore extending our framework to tackle additional emerging models in graph learning.

Acknowledgements

This work was supported in part by Sichuan Youth Science and Technology Innovation Team (Grant Nos. 2022JDTD0014, 2021JDJQ0036). The work of Zhiguo Wang was supported in part by the National Natural Science Foundation of China under Grant 62203313.

References

- [1] Antonio Ortega, Pascal Frossard, Jelena Kovačević, José MF Moura, and Pierre Vandergheynst. Graph signal processing: Overview, challenges, and applications. *Proceedings of the IEEE*, 106(5):808–828, 2018.
- [2] Xiaowen Dong, Dorina Thanou, Laura Toni, Michael Bronstein, and Pascal Frossard. Graph signal processing for machine learning: A review and new perspectives. *IEEE Signal Processing Magazine*, 37(6):117–127, 2020.
- [3] Santo Fortunato, Carl T Bergstrom, Katy Börner, James A Evans, Dirk Helbing, Staša Milojević, Alexander M Petersen, Filippo Radicchi, Roberta Sinatra, Brian Uzzi, et al. Science of science. *Science*, 359(6379):eaao0185, 2018.
- [4] Xiaozou Zhang, Yang Gao, Yang Liu, Yujia Zhu, Peng Zhang, Chuan Zhou, Qingyun Liu, and Hongyang Chen. Meta structure search for link weight prediction in heterogeneous graphs. In *Proceedings of IEEE ICASSP*, pages 5195–5199, 2024.
- [5] Jiaying Liu, Jing Ren, Wenqing Zheng, Lianhua Chi, Ivan Lee, and Feng Xia. Web of scholars: A scholar knowledge graph. In *Proceedings of the 43rd International ACM SIGIR Conference on Research and Development in Information Retrieval*, pages 2153–2156, 2020.
- [6] Jiaying Liu, Feng Xia, Lei Wang, Bo Xu, Xiangjie Kong, Hanghang Tong, and Irwin King. Shifu2: A network representation learning based model for advisor-advisee relationship mining. *IEEE Transactions on Knowledge and Data Engineering*, 33(4):1763–1777, 2019.

[7] David I Shuman, Sunil K Narang, Pascal Frossard, Antonio Ortega, and Pierre Vandergheynst. The emerging field of signal processing on graphs: Extending high-dimensional data analysis to networks and other irregular domains. *IEEE Signal Processing Magazine*, 30(3):83–98, 2013.

[8] Kai Qiu, Xianghui Mao, Xinyue Shen, Xiaohan Wang, Tiejian Li, and Yuantao Gu. Time-varying graph signal reconstruction. *IEEE Journal of Selected Topics in Signal Processing*, 11(6):870–883, 2017.

[9] Hilmi E Egilmez, Eduardo Pavez, and Antonio Ortega. Graph learning from data under Laplacian and structural constraints. *IEEE Journal of Selected Topics in Signal Processing*, 11(6):825–841, 2017.

[10] Petar Djuric and Cédric Richard. *Cooperative and graph signal processing: Principles and applications*. Academic Press, 2018.

[11] Vassilis Kalofolias. How to learn a graph from smooth signals. In *Artificial Intelligence and Statistics*, pages 920–929. PMLR, 2016.

[12] Aliaksei Sandryhaila and José M. F. Moura. Discrete signal processing on graphs. *IEEE Transactions on Signal Processing*, 61(7):1644–1656, 2013.

[13] David I Shuman, Sunil K. Narang, Pascal Frossard, Antonio Ortega, and Pierre Vandergheynst. The emerging field of signal processing on graphs: Extending high-dimensional data analysis to networks and other irregular domains. *IEEE Signal Processing Magazine*, 30(3):83–98, 2013.

[14] Wenling Li, Yingmin Jia, and Junping Du. Resilient filtering for nonlinear complex networks with multiplicative noise. *IEEE Transactions on Automatic Control*, 64(6):2522–2528, 2018.

[15] Shiqian Ma. Alternating proximal gradient method for convex minimization. *Journal of Scientific Computing*, 68(2):546–572, 2016.

[16] Xiaolu Wang, Chaorui Yao, and Anthony Man-Cho So. A linearly convergent optimization framework for learning graphs from smooth signals. *IEEE Transactions on Signal and Information Processing over Networks*, 2023.

[17] Shi-Yuk Fong and Anthony Man-Cho So. An efficient optimization framework for learning general signed graphs from smooth signals. In *2024 IEEE 13rd Sensor Array and Multichannel Signal Processing Workshop (SAM)*, pages 1–5, 2024.

[18] Xiaolu Wang, Chaorui Yao, Haoyu Lei, and Anthony Man-Cho So. An efficient alternating direction method for graph learning from smooth signals. In *Proceedings of IEEE ICASSP*, pages 5380–5384, 2021.

[19] Santiago Segarra, Antonio G Marques, Gonzalo Mateos, and Alejandro Ribeiro. Network topology inference from spectral templates. *IEEE Transactions on Signal and Information Processing over Networks*, 3(3):467–483, 2017.

[20] Eric D Kolaczyk and Gábor Csárdi. *Statistical analysis of network data with R*, volume 65. Springer, 2014.

[21] Yupeng Chen, Zhiguo Wang, and Xiaojing Shen. An unbiased symmetric matrix estimator for topology inference under partial observability. *IEEE Signal Processing Letters*, 29:1257–1261, 2022.

[22] Saurav Talukdar, Deepjyoti Deka, Harish Doddi, Donatello Materassi, Michael Chertkov, and Murti V Salapaka. Physics informed topology learning in networks of linear dynamical systems. *Automatica*, 112:108705, 2020.

[23] Mishfad Shaikh Veedu and Murti V Salapaka. Topology identification under spatially correlated noise. *Automatica*, 156:111182, 2023.

[24] Yushan Li, Jianping He, Cailian Chen, and Xinpeng Guan. Topology inference for network systems: Causality perspective and non-asymptotic performance. *IEEE Transactions on Automatic Control*, 2023.

[25] Georgios V Karanikolas, Georgios B Giannakis, Konstantinos Slavakis, and Richard M Leahy. Multi-kernel based nonlinear models for connectivity identification of brain networks. In *Proceedings of IEEE ICASSP*, pages 6315–6319, 2016.

[26] Yanning Shen, Brian Baingana, and Georgios B Giannakis. Kernel-based structural equation models for topology identification of directed networks. *IEEE Transactions on Signal Processing*, 65(10):2503–2516, 2017.

[27] Wenwu Yu, Hongzhe Liu, Wei Xing Zheng, and Yanan Zhu. Distributed discrete-time convex optimization with nonidentical local constraints over time-varying unbalanced directed graphs. *Automatica*, 134:109899, 2021.

[28] Fenxiao Chen, Yun-Cheng Wang, Bin Wang, and C-C Jay Kuo. Graph representation learning: A survey. *APSIPA Transactions on Signal and Information Processing*, 9:e15, 2020.

[29] Xing Su, Shan Xue, Fanzhen Liu, Jia Wu, Jian Yang, Chuan Zhou, Wenbin Hu, Cecile Paris, Surya Nepal, Di Jin, et al. A comprehensive survey on community detection with deep learning. *IEEE Transactions on Neural Networks and Learning Systems*, 2022.

[30] Nurul A Asif, Yeahia Sarker, Ripon K Chakrabortty, Michael J Ryan, Md Hafiz Ahamed, Dip K Saha, Faisal R Badal, Sajal K Das, Md Firoz Ali, Sumaya I Moyeen, et al. Graph neural network: A comprehensive review on non-euclidean space. *IEEE Access*, 9:60588–60606, 2021.

[31] Zonghan Wu, Shirui Pan, Fengwen Chen, Guodong Long, Chengqi Zhang, and S Yu Philip. A comprehensive survey on graph neural networks. *IEEE Transactions on Neural Networks and Learning Systems*, 32(1):4–24, 2020.

[32] Simon Geisler, Tobias Schmidt, Hakan Sirin, Daniel Zügner, Aleksandar Bojchevski, and Stephan Günnemann. Robustness of graph neural networks at scale. *Advances in Neural Information Processing Systems*, 34:7637–7649, 2021.

[33] Jie Zhou, Ganqu Cui, Shengding Hu, Zhengyan Zhang, Cheng Yang, Zhiyuan Liu, Lifeng Wang, Changcheng Li, and Maosong Sun. Graph neural networks: A review of methods and applications. *AI Open*, 1:57–81, 2020.

[34] Andrei Buculea, Samuel Rey, and Antonio G Marques. Learning graphs from smooth and graph-stationary signals with hidden variables. *IEEE Transactions on Signal and Information Processing over Networks*, 8:273–287, 2022.

[35] Venkat Chandrasekaran, Pablo A Parrilo, and Alan S Willsky. Latent variable graphical model selection via convex optimization. In *Proceedings of IEEE Allerton*, pages 1610–1613, 2010.

[36] Manuel Hentschel, Sebastian Engelke, and Johan Segers. Statistical inference for hüsler-reiss graphical models through matrix completions. *Journal of the American Statistical Association*, pages 1–25, 2024.

[37] Jonathan Mei and José MF Moura. Silvar: Single index latent variable models. *IEEE Transactions on Signal Processing*, 66(11):2790–2803, 2018.

[38] Madeline Navarro, Samuel Rey, Andrei Buculea, Antonio G. Marques, and Santiago Segarra. Joint network topology inference in the presence of hidden nodes. *IEEE Transactions on Signal Processing*, 72:2710–2725, 2024.

[39] Mingyi Hong and Zhi-Quan Luo. On the linear convergence of the alternating direction method of multipliers. *Mathematical Programming*, 162(1):165–199, 2017.

[40] Vincenzo Matta, Augusto Santos, and Ali H Sayed. Graph learning over partially observed diffusion networks: Role of degree concentration. *IEEE Open Journal of Signal Processing*, 3:335–371, 2022.

[41] Neal Parikh, Stephen Boyd, et al. Proximal algorithms. *Foundations and trends® in Optimization*, 1(3):127–239, 2014.

[42] Amir Beck. *First-order methods in optimization*. SIAM, 2017.

[43] Wei Hong Yang and Deren Han. Linear convergence of the alternating direction method of multipliers for a class of convex optimization problems. *SIAM Journal on Numerical Analysis*, 54(2):625–640, 2016.

[44] Deren Han, Defeng Sun, and Liwei Zhang. Linear rate convergence of the alternating direction method of multipliers for convex composite programming. *Mathematics of Operations Research*, 43(2):622–637, 2018.

[45] Xiaowen Dong, Dorina Thanou, Pascal Frossard, and Pierre Vandergheynst. Learning Laplacian matrix in smooth graph signal representations. *IEEE Transactions on Signal Processing*, 64(23):6160–6173, 2016.

[46] Rion Brattig Correia, Luciana P de Araújo Kohler, Mauro M Mattos, and Luis M Rocha. City-wide electronic health records reveal gender and age biases in administration of known drug–drug interactions. *NPJ Digital Medicine*, 2(1):74, 2019.

[47] M. E. J. Newman. Finding community structure in networks using the eigenvectors of matrices. *Physical Review E—Statistical, Nonlinear, and Soft Matter Physics*, 74:036104, Sep 2006.

[48] Kerrianne Ryan, Zhiyuan Lu, and Ian A Meinertzhagen. The CNS connectome of a tadpole larva of *Ciona intestinalis* (L.) highlights sidedness in the brain of a chordate sibling. *Elife*, 5:e16962, 2016.

[49] Michael Grant and Stephen Boyd. CVX: Matlab software for disciplined convex programming, version 2.1, 2014.

[50] Haibin Zhang, Jiaoqiao Jiang, and Zhi-Quan Luo. On the linear convergence of a proximal gradient method for a class of nonsmooth convex minimization problems. *Journal of the Operations Research Society of China*, 1(2):163–186, 2013.

[51] Seyed Saman Saboksayr, Gonzalo Mateos, and Mujdat Cetin. Online discriminative graph learning from multi-class smooth signals. *Signal Processing*, 186:108101, 2021.

A Proof of Proposition 1

Proof. Note that $f_1(\mathbf{w}) = \frac{1}{2}\mathbf{z}^T \mathbf{w} + \beta \|\mathbf{w}\|_2^2 + \mathbb{I}_{\mathbb{R}_+^p}(\mathbf{w})$, and

$$\begin{aligned} \text{prox}_{\tau_1 f_1}(\mathbf{w}) &= \arg \min_{\mathbf{x}} \left\{ f_1(\mathbf{x}) + \frac{1}{2\tau_1} \|\mathbf{x} - \mathbf{w}\|_2^2 \right\} \\ &= \arg \min_{\mathbf{x}} \left\{ \frac{1}{2}\mathbf{z}^T \mathbf{x} + \beta \|\mathbf{x}\|_2^2 + \mathbb{I}_{\mathbb{R}_+^p}(\mathbf{x}) + \frac{1}{2\tau_1} \|\mathbf{x} - \mathbf{w}\|_2^2 \right\} \\ &= \max \left\{ \frac{\mathbf{w} - \frac{1}{2}\tau_1 \mathbf{z}}{2\tau_1 \beta + 1}, \mathbf{0} \right\}, \end{aligned}$$

where $\max\{\mathbf{a}, \mathbf{0}\}$ denotes the element-wise maximum of \mathbf{a} and $\mathbf{0}$. This completes the proof. \square

B Proof of Proposition 4

Proof. Note that $f_3(\mathbf{k}) = 2\mathbf{b}^T \mathbf{k} + \gamma_{2,1} h(\mathbf{k})$, where $h(\mathbf{k}) = \|\tilde{\mathbf{K}}\|_{2,1}$, and combining Lemma 3, we have

$$\begin{aligned} \text{prox}_{\tau_3 f_3}(\mathbf{k}) &= \arg \min_{\mathbf{x}} \left\{ f_3(\mathbf{x}) + \frac{1}{2\tau_3} \|\mathbf{x} - \mathbf{k}\|_2^2 \right\} \\ &= \arg \min_{\mathbf{x}} \left\{ 2\mathbf{b}^T \mathbf{x} + \gamma_{2,1} \|\tilde{\mathbf{X}}\|_{2,1} + \frac{1}{2\tau_3} \|\mathbf{x} - \mathbf{k}\|_2^2 \right\} \\ &= \left[1 - \frac{\tau_3 \gamma_{2,1}}{\|\mathbf{k} - 2\tau_3 \mathbf{b}\|_2} \right]_+ (\mathbf{k} - 2\tau_3 \mathbf{b}). \end{aligned}$$

This completes the proof. \square

C Proof of Proposition 5

Proof. Note that $f_4(\mathbf{v}) = \mathbf{d}^T \mathbf{v} + \mathbb{I}_{\mathbb{R}_+}(\mathbf{v})$, thus, we have

$$\begin{aligned} \text{prox}_{\tau_4 f_4}(\mathbf{v}) &= \arg \min_{\mathbf{x}} \left\{ f_4(\mathbf{x}) + \frac{1}{2\tau_4} \|\mathbf{x} - \mathbf{v}\|_2^2 \right\} \\ &= \arg \min_{\mathbf{x}} \left\{ \mathbf{d}^T \mathbf{x} + \mathbb{I}_{\mathbb{R}_+}(\mathbf{x}) + \frac{1}{2\tau_4} \|\mathbf{x} - \mathbf{v}\|_2^2 \right\} \\ &= \max\{\mathbf{v} - \tau_4 \mathbf{d}, \mathbf{0}\}. \end{aligned}$$

This completes the proof. \square

D Proof of Theorem 7

Proof. Our Theorem 8 is a direct derivation of [39]. The main convergence result, Theorem 3.1 in [39], is based on Assumption (a)-(g) in [39]. So, to prove our Theorem 8, we only need to verify whether our Problem (11) satisfies these assumptions.

First, it is easy to verify that Problem (11) meets Assumption (a), (c), (d) and (e). And next, Assumption (b) in [39] says that $f(\mathbf{x}) = f_1(\mathbf{x}_1) + \dots + f_K(\mathbf{x}_K)$, with each f_k further decomposable as

$$f_k(\mathbf{x}_k) = g_k(\mathbf{A}_k \mathbf{x}_k) + h(\mathbf{x}_k). \quad (\text{D.1})$$

Although our f_i , $i = 1, 2, 3, 4$ only consist of the convex function f_i , this does not contradict Equation (D.1), for the strictly convex part being effectively absent by having $\mathbf{A}_k = \mathbf{0}$.

And then, for Assumption (f), although our matrix \mathbf{A} does not have full rank, like the discussion at Section 4.1 in [39], our algorithms align with linearized proximal ADMM framework rather the classic ADMM framework. Thus, without requiring the full rankness of \mathbf{A} , we can still establish the linear convergence of our GLOPSS-CS and GLOPSS-LR.

Last but not least, let $\mathbf{X} = X_1 \times X_2 \times X_3 \times X_4$ be the feasible set of Problem (11), with $\mathbf{w} \in X_1$, $\mathbf{u} \in X_2$, $\mathbf{k} \in X_3$, and $\mathbf{v} \in X_4$. For Assumption (g), it is easy to verify that the feasible sets X_i , $i = 1, 2, 3, 4$ are compact polyhedral sets, which are needed to ensure that certain error bound of the primal and dual problem of (11) hold. For example, for Algorithm 1, $f_3(\mathbf{k})$ includes the group LASSO penalization $\|\cdot\|_{2,1}$, the proof of error bound of this type of function can be found in [50].

Thus, we have verified that Problem (11) meets all the conditions listed in Assumption (a)–(g) in [39], hence the linear convergence result can be obtained. This completes the proof of Theorem 8. \square

E Proof of Theorem 8

Proof. Since $(\mathbf{w}^*, \mathbf{u}^*, \mathbf{k}^*, \mathbf{v}^*, \lambda^*)$ is optimal to (11), it follows from the KKT conditions that the following hold:

$$\mathbf{0} \in \partial f_1(\mathbf{w}^*) - \mathbf{M}_1^T \lambda^*, \quad (\text{E.1})$$

$$\mathbf{0} \in \partial f_2(\mathbf{u}^*) - \mathbf{M}_2^T \lambda^*, \quad (\text{E.2})$$

$$\mathbf{0} \in \partial f_3(\mathbf{k}^*) - \mathbf{M}_3^T \lambda^*, \quad (\text{E.3})$$

$$\mathbf{0} \in \partial f_4(\mathbf{v}^*) - \mathbf{M}_4^T \lambda^*, \quad (\text{E.4})$$

$$\mathbf{0} = \mathbf{A}\mathbf{x}. \quad (\text{E.5})$$

Note that the optimality conditions for the first subproblem (i.e., the subproblem with respect to \mathbf{w}) in Algorithm 1 is given by

$$\begin{aligned} \mathbf{0} \in & \frac{\tau_1}{\rho} \partial f_1(\mathbf{w}^{i+1}) + \mathbf{w}^{i+1} - \mathbf{w}^i \\ & + \tau_1 \mathbf{M}_1^T (\mathbf{M}_1 \mathbf{w}^i + \mathbf{M}_2 \mathbf{u}^i + \mathbf{M}_3 \mathbf{k}^i + \mathbf{M}_4 \mathbf{v}^i - \frac{\lambda^i}{\rho}). \end{aligned} \quad (\text{E.6})$$

By using the updating formula for λ^i , i.e.,

$$\lambda^{i+1} = \lambda^i - \rho \mathbf{A}\mathbf{x}^{i+1}, \quad (\text{E.7})$$

(E.6) can be reduced to

$$\begin{aligned} \mathbf{0} \in & \frac{\tau_1}{\rho} \partial f_1(\mathbf{w}^{i+1}) + \mathbf{w}^{i+1} - \mathbf{w}^i + \tau_1 \mathbf{M}_1^T (\mathbf{M}_1(\mathbf{w}^i - \mathbf{w}^{i+1}) \\ & + \mathbf{M}_2(\mathbf{u}^i - \mathbf{u}^{i+1}) + \mathbf{M}_3(\mathbf{k}^i - \mathbf{k}^{i+1}) + \mathbf{M}_4(\mathbf{v}^i - \mathbf{v}^{i+1}) \\ & - \frac{\lambda^{i+1}}{\rho}). \end{aligned} \quad (\text{E.8})$$

Combining (E.1) and (E.8) and using the fact that $\partial f_1(\cdot)$ is a monotone operator, we get

$$\begin{aligned} & (\mathbf{w}^{i+1} - \mathbf{w}^*)^T (\frac{\rho}{\tau_1} (\mathbf{w}^i - \mathbf{w}^{i+1}) - \rho \mathbf{M}_1^T \mathbf{M}_1 (\mathbf{w}^i - \mathbf{w}^{i+1}) \\ & - \rho \mathbf{M}_1^T (\mathbf{M}_2(\mathbf{u}^i - \mathbf{u}^{i+1}) + \mathbf{M}_3(\mathbf{k}^i - \mathbf{k}^{i+1}) \\ & + \mathbf{M}_4(\mathbf{v}^i - \mathbf{v}^{i+1})) + \mathbf{M}_1^T (\lambda^{i+1} - \lambda^*)) \geq \mathbf{0}. \end{aligned} \quad (\text{E.9})$$

The optimality conditions for the second subproblem (i.e., the subproblem with respect to \mathbf{u}) in Algorithm 1 are given by

$$\begin{aligned} \mathbf{0} \in & \frac{\tau_2}{\rho} \partial f_2(\mathbf{u}^{i+1}) + \mathbf{u}^{i+1} - \mathbf{u}^i \\ & + \tau_2 \mathbf{M}_2^T (\mathbf{M}_1 \mathbf{w}^{i+1} + \mathbf{M}_2 \mathbf{u}^i + \mathbf{M}_3 \mathbf{k}^i + \mathbf{M}_4 \mathbf{v}^i - \frac{\lambda^i}{\rho}). \end{aligned} \quad (\text{E.10})$$

Using (E.7), (E.10) can be reduced to

$$\begin{aligned} \mathbf{0} \in & \frac{\tau_2}{\rho} \partial f_2(\mathbf{u}^{i+1}) + \mathbf{u}^{i+1} - \mathbf{u}^i + \tau_2 \mathbf{M}_2^T (\mathbf{M}_1 \mathbf{w}^{i+1} \\ & + \mathbf{M}_2 \mathbf{u}^i + \mathbf{M}_3 \mathbf{k}^i + \mathbf{M}_4 \mathbf{v}^i - \frac{\lambda^i}{\rho}). \end{aligned} \quad (\text{E.11})$$

Combining (E.2) and (11) and using the fact that $\partial f_2(\cdot)$ is a monotone operator, we get

$$\begin{aligned} & (\mathbf{u}^{i+1} - \mathbf{u}^*)^T (\frac{\rho}{\tau_2} (\mathbf{u}^i - \mathbf{u}^{i+1}) - \rho \mathbf{M}_2^T \mathbf{M}_2 (\mathbf{u}^i - \mathbf{u}^{i+1}) \\ & - \mathbf{M}_2^T (\mathbf{M}_3(\mathbf{k}^i - \mathbf{k}^{i+1}) + \mathbf{M}_4(\mathbf{v}^i - \mathbf{v}^{i+1})) \\ & + \mathbf{M}_2^T (\lambda^{i+1} - \lambda^*)) \geq \mathbf{0}. \end{aligned} \quad (\text{E.12})$$

Similarly, for \mathbf{k} and \mathbf{v} , we respectively have

$$\begin{aligned} & (\mathbf{k}^{i+1} - \mathbf{k}^*)^T (\frac{\rho}{\tau_3} (\mathbf{k}^i - \mathbf{k}^{i+1}) - \rho \mathbf{M}_3^T \mathbf{M}_3 (\mathbf{k}^i - \mathbf{k}^{i+1}) \\ & - \mathbf{M}_3^T (\mathbf{M}_4(\mathbf{v}^i - \mathbf{v}^{i+1})) + \mathbf{M}_2^T (\lambda^{i+1} - \lambda^*)) \geq \mathbf{0} \end{aligned} \quad (\text{E.13})$$

and

$$\begin{aligned} & (\mathbf{v}^{i+1} - \mathbf{v}^*)^T (\frac{\rho}{\tau_4} (\mathbf{v}^i - \mathbf{v}^{i+1}) - \rho \mathbf{M}_4^T \mathbf{M}_4 (\mathbf{v}^i - \mathbf{v}^{i+1}) \\ & + \mathbf{M}_4^T (\lambda^{i+1} - \lambda^*)) \geq \mathbf{0}. \end{aligned} \quad (\text{E.14})$$

Summing (E.9), (E.12), (E.13) and (E.14), by using $\mathbf{A}\mathbf{x}^* = \mathbf{0}$, we obtain

$$\begin{aligned} & (\mathbf{w}^{i+1} - \mathbf{w}^*)^T (\frac{\rho}{\tau_1} \mathbf{I} - \rho \mathbf{M}_1^T \mathbf{M}_1) (\mathbf{w}^i - \mathbf{w}^{i+1}) \\ & + (\mathbf{u}^{i+1} - \mathbf{u}^*)^T (\frac{\rho}{\tau_2} \mathbf{I} - \rho \mathbf{M}_2^T \mathbf{M}_2) (\mathbf{u}^i - \mathbf{u}^{i+1}) \\ & + (\mathbf{k}^{i+1} - \mathbf{k}^*)^T (\frac{\rho}{\tau_3} \mathbf{I} - \rho \mathbf{M}_3^T \mathbf{M}_3) (\mathbf{k}^i - \mathbf{k}^{i+1}) \\ & + \frac{\rho}{\tau_4} (\mathbf{v}^{i+1} - \mathbf{v}^*)^T (\mathbf{v}^i - \mathbf{v}^{i+1}) \\ & - (\lambda^i - \lambda^{i+1})^T \mathbf{M}_4 (\mathbf{v}^i - \mathbf{v}^{i+1}) \\ & + \frac{1}{\rho} (\lambda^i - \lambda^{i+1})^T (\lambda^{i+1} - \lambda^*) \geq \mathbf{0}. \end{aligned} \quad (\text{E.15})$$

Using the notation of \mathbf{y}^i , \mathbf{y}^* and $\mathbf{M} = \text{Diag}[\frac{\rho}{\tau_1} \mathbf{I} - \rho \mathbf{M}_1^T \mathbf{M}_1; \frac{\rho}{\tau_2} \mathbf{I} - \rho \mathbf{M}_2^T \mathbf{M}_2; \frac{\rho}{\tau_3} \mathbf{I} - \rho \mathbf{M}_3^T \mathbf{M}_3; \frac{\rho}{\tau_4} \mathbf{I}; \frac{1}{\rho} \mathbf{I}]$, (E.15)

can be written as

$$\langle \mathbf{y}^{i+1} - \mathbf{y}^*, \mathbf{y}^i - \mathbf{y}^{i+1} \rangle_{\mathbf{M}} \geq \langle \lambda^i - \lambda^{i+1}, \mathbf{M}_4 \mathbf{v}^i - \mathbf{M}_4 \mathbf{v}^{i+1} \rangle, \quad (\text{E.16})$$

which can be further written as

$$\begin{aligned} \langle \mathbf{y}^i - \mathbf{y}^*, \mathbf{y}^i - \mathbf{y}^{i+1} \rangle_{\mathbf{M}} &\geq \|\mathbf{y}^i - \mathbf{y}^{i+1}\|_{\mathbf{M}}^2 \\ &+ \langle \lambda^i - \lambda^{i+1}, \mathbf{M}_4 \mathbf{v}^i - \mathbf{M}_4 \mathbf{v}^{i+1} \rangle. \end{aligned} \quad (\text{E.17})$$

Combining (E.17) with the identity

$$\begin{aligned} \|\mathbf{y}^{i+1} - \mathbf{y}^*\|_{\mathbf{M}}^2 &= \|\mathbf{y}^{i+1} - \mathbf{y}^i\|_{\mathbf{M}}^2 - 2\langle \mathbf{y}^i - \mathbf{y}^{i+1}, \mathbf{y}^i - \mathbf{y}^* \rangle_{\mathbf{M}} \\ &+ \|\mathbf{y}^i - \mathbf{y}^*\|_{\mathbf{M}}^2, \end{aligned} \quad (\text{E.18})$$

we get

$$\begin{aligned} \|\mathbf{y}^i - \mathbf{y}^*\|_{\mathbf{M}}^2 - \|\mathbf{y}^{i+1} - \mathbf{y}^*\|_{\mathbf{M}}^2 &= 2\langle \mathbf{y}^i - \mathbf{y}^{i+1}, \mathbf{y}^i - \mathbf{y}^* \rangle_{\mathbf{M}} - \|\mathbf{y}^{i+1} - \mathbf{y}^i\|_{\mathbf{M}}^2 \\ &\geq \|\mathbf{y}^i - \mathbf{y}^{i+1}\|_{\mathbf{M}}^2 + 2\langle \lambda^i - \lambda^{i+1}, \mathbf{M}_4 \mathbf{v}^i - \mathbf{M}_4 \mathbf{v}^{i+1} \rangle. \end{aligned} \quad (\text{E.19})$$

Let $\xi := \frac{1}{2} + \frac{\tau_4 \sigma_{\max}^2(\mathbf{M}_4)}{2}$, then we know that $\tau_4 \sigma_{\max}^2(\mathbf{M}_4) < \xi < 1$ since $\tau_4 < \frac{1}{\sigma_{\max}^2(\mathbf{M}_4)}$. Let $\mu := \frac{\xi}{\rho}$. Then from the Cauchy-Schwartz inequality we have

$$\begin{aligned} 2\langle \lambda^i - \lambda^{i+1}, \mathbf{M}_4 \mathbf{v}^i - \mathbf{M}_4 \mathbf{v}^{i+1} \rangle &\geq -\mu \|\lambda^i - \lambda^{i+1}\|^2 - \frac{1}{\mu} \|\mathbf{M}_4 \mathbf{v}^i - \mathbf{M}_4 \mathbf{v}^{i+1}\|^2 \\ &\geq -\mu \|\lambda^i - \lambda^{i+1}\|^2 - \frac{1}{\mu} \sigma_{\max}^2(\mathbf{M}_4) \|\mathbf{M}_4 \mathbf{v}^i - \mathbf{M}_4 \mathbf{v}^{i+1}\|^2. \end{aligned} \quad (\text{E.20})$$

Combining (E.19) and (E.20) we get

$$\begin{aligned} \|\mathbf{y}^i - \mathbf{y}^*\|_{\mathbf{M}}^2 - \|\mathbf{y}^{i+1} - \mathbf{y}^*\|_{\mathbf{M}}^2 &\geq (\mathbf{w}^i - \mathbf{w}^{i+1})^T \left(\frac{\rho}{\tau_1} \mathbf{I} - \rho \mathbf{M}_1^T \mathbf{M}_1 \right) (\mathbf{w}^i - \mathbf{w}^{i+1}) \\ &+ (\mathbf{u}^i - \mathbf{u}^{i+1})^T \left(\frac{\rho}{\tau_2} \mathbf{I} - \rho \mathbf{M}_2^T \mathbf{M}_2 \right) (\mathbf{u}^i - \mathbf{u}^{i+1}) \\ &+ (\mathbf{k}^i - \mathbf{k}^{i+1})^T \left(\frac{\rho}{\tau_3} \mathbf{I} - \rho \mathbf{M}_3^T \mathbf{M}_3 \right) (\mathbf{k}^i - \mathbf{k}^{i+1}) \\ &+ \left(\frac{\rho}{\tau_4} - \frac{1}{\mu} \sigma_{\max}^2(\mathbf{M}_4) \right) \|\mathbf{v}^i - \mathbf{v}^{i+1}\|^2 \\ &+ \left(\frac{1}{\rho} - \mu \right) \|\lambda^i - \lambda^{i+1}\|^2 \\ &\geq c \|\mathbf{y}^i - \mathbf{y}^{i+1}\|_{\mathbf{M}}^2, \end{aligned} \quad (\text{E.21})$$

where $c := \min\left\{ \frac{\rho}{\tau_1} - \rho \sigma_{\max}^2(\mathbf{M}_1), \frac{\rho}{\tau_2} - \frac{1}{\mu} \sigma_{\max}^2(\mathbf{M}_2), \frac{\rho}{\tau_3} - \rho \sigma_{\max}^2(\mathbf{M}_3), \frac{\rho}{\tau_4} - \rho \sigma_{\max}^2(\mathbf{M}_4), \frac{1}{\rho} - \mu \right\} > 0$. This completes the proof. \square

F Proof of Proposition 9

Proof. We have $\mathbf{M}_4 = \begin{bmatrix} \mathbf{a}^T \\ \mathbf{0} \end{bmatrix}$. It is easy to have $\|\mathbf{M}_4\|_2 = 2$.

Next, we have $\mathbf{M}_3 = [2\mathbf{b}^T; \mathbf{0}]$, so we get

$$\mathbf{M}_3 \mathbf{M}_3^T = \begin{bmatrix} 4\mathbf{b}^T \mathbf{b} & \mathbf{0} \\ \mathbf{0} & \mathbf{0} \end{bmatrix},$$

It is easy to have $\|\mathbf{M}_3\|_2 = 2\sqrt{o}$. And then, we know $\mathbf{M}_2 = [\mathbf{0}; -\mathbf{I}]$, so we get $\|\mathbf{M}_2\|_2 = 1$. Lastly, we have

$\mathbf{M}_1 = \begin{bmatrix} \frac{1}{2} \mathbf{z}^T \\ \mathbf{B} \end{bmatrix}$. To bound $\|\mathbf{M}_1\|_2$, we have

$$\|\mathbf{M}_1\|_2 \leq \frac{1}{2} \|\mathbf{z}\|_2 + \|\mathbf{B}\|_2 \quad (\text{F.1})$$

It is shown in [51] that $\|\mathbf{B}\|_2 = \sqrt{2(o-1)}$. By the Gershgorin circle theorem, denoting $\kappa := \max_{ij} z_{ij}$, we have

$$\lambda(\mathbf{z} \mathbf{z}^T) \leq \kappa^2 o^2, \quad (\text{F.2})$$

Combining (F.1) and (F.2), gives

$$\|\mathbf{M}_1\|_2 \leq \frac{1}{2} \kappa o + \sqrt{2(o-1)} \quad (\text{F.3})$$

This complete the proof. \square

G Proof of Lemma 11

Proof. By (15), there exists $\bar{\mathbf{w}} \in \partial f_1(\mathbf{w}^{i+1})$ such that

$$\begin{aligned} \mathbf{w}^{i+1} &= P_{X_1}(\mathbf{w}^{i+1} - [\bar{\mathbf{w}} + \frac{\rho}{\tau_1}(\mathbf{w}^{i+1} \\ &- (\mathbf{w}^i - \tau_1 \mathbf{M}_1^T (\mathbf{M}_1 \mathbf{w}^i + \mathbf{M}_2 \mathbf{u}^i \\ &+ \mathbf{M}_3 \mathbf{k}^i + \mathbf{M}_4 \mathbf{v}^i - \frac{\lambda^i}{\rho})))]), \end{aligned} \quad (\text{G.1})$$

Using the above relation, we can obtain that

$$\begin{aligned}
& \text{dist}(\mathbf{0}, \mathcal{E}_{\mathbf{w}}(\mathbf{y}^{i+1})) \\
&= \text{dist}(\mathbf{w}^{i+1}, P_{X_1}(\mathbf{w}^{i+1} - (\partial f_1(\mathbf{w}^{i+1}) - \mathbf{M}_1^T \lambda^{i+1}))) \\
&\leq \|P_{X_1}(\mathbf{w}^{i+1} - [\bar{\mathbf{w}} + \frac{\rho}{\tau_1}(\mathbf{w}^{i+1} - (\mathbf{w}^i - \tau_1 \mathbf{M}_1^T (\mathbf{M}_1 \mathbf{w}^i \\
&\quad + \mathbf{M}_2 \mathbf{u}^i + \mathbf{M}_3 \mathbf{k}^i + \mathbf{M}_4 \mathbf{v}^i - \frac{\lambda^i}{\rho})))])]) \\
&\quad - P_{X_1}(\mathbf{w}^{i+1} - (\bar{\mathbf{w}} - \mathbf{M}_1^T \lambda^{i+1}))\| \\
&\leq \|\frac{\rho}{\tau_1}(\mathbf{w}^{i+1} - \mathbf{w}^i) + \rho \mathbf{M}_1^T (\mathbf{M}_1 \mathbf{w}^i + \mathbf{M}_2 \mathbf{u}^i + \mathbf{M}_3 \mathbf{k}^i \\
&\quad + \mathbf{M}_4 \mathbf{v}^i) + \mathbf{M}_1^T (\lambda^{i+1} - \lambda^i)\| \\
&= \|\frac{\rho}{\tau_1}(\mathbf{w}^{i+1} - \mathbf{w}^i) + \rho \mathbf{M}_1^T [\mathbf{M}_1(\mathbf{w}^i - \mathbf{w}^{i+1}) \\
&\quad + \mathbf{M}_2(\mathbf{u}^i - \mathbf{u}^{i+1}) + \mathbf{M}_3(\mathbf{k}^i - \mathbf{k}^{i+1}) + \mathbf{M}_4(\mathbf{v}^i - \mathbf{v}^{i+1})]\| \\
&\leq \|\frac{\rho}{\tau_1} \mathbf{I} - \rho \mathbf{M}_1^T \mathbf{M}_1\| \|\mathbf{w}^{i+1} - \mathbf{w}^i\| \\
&\quad + \rho \|\mathbf{M}_1^T \mathbf{M}_2\| \|\mathbf{u}^{i+1} - \mathbf{u}^i\| + \rho \|\mathbf{M}_1^T \mathbf{M}_3\| \|\mathbf{k}^{i+1} - \mathbf{k}^i\| \\
&\quad + \rho \|\mathbf{M}_1^T \mathbf{M}_4\| \|\mathbf{v}^{i+1} - \mathbf{v}^i\|, \tag{G.2}
\end{aligned}$$

where the second equality holds due to the update formula of λ^i in (23).

By (17), there exists $\bar{\mathbf{u}} \in \partial f_2(\mathbf{u}^{i+1})$ such that

$$\begin{aligned}
\mathbf{u}^{i+1} &= P_{X_2}(\mathbf{u}^{i+1} - [\bar{\mathbf{u}} + \frac{\rho}{\tau_2}(\mathbf{u}^{i+1} \\
&\quad - (\mathbf{u}^i - \tau_2 \mathbf{M}_1^T (\mathbf{M}_1 \mathbf{w}^{i+1} + \mathbf{M}_2 \mathbf{u}^i \\
&\quad + \mathbf{M}_3 \mathbf{k}^i + \mathbf{M}_4 \mathbf{v}^i - \frac{\lambda^i}{\rho})))])]. \tag{G.3}
\end{aligned}$$

Then, like (G.2), we have

$$\begin{aligned}
& \text{dist}(\mathbf{0}, \mathcal{E}_{\mathbf{u}}(\mathbf{y}^{i+1})) \\
&= \text{dist}(\mathbf{u}^{i+1}, P_{X_2}(\mathbf{u}^{i+1} - (\partial f_2(\mathbf{u}^{i+1}) - \mathbf{M}_2^T \lambda^{i+1}))) \\
&\leq \|P_{X_2}(\mathbf{u}^{i+1} - [\bar{\mathbf{u}} + \frac{\rho}{\tau_2}(\mathbf{u}^{i+1} - (\mathbf{u}^i - \tau_2 \mathbf{M}_2^T (\mathbf{M}_1 \mathbf{w}^{i+1} \\
&\quad + \mathbf{M}_2 \mathbf{u}^i + \mathbf{M}_3 \mathbf{k}^i + \mathbf{M}_4 \mathbf{v}^i - \frac{\lambda^i}{\rho})))])]) \\
&\quad - P_{X_2}(\mathbf{u}^{i+1} - (\bar{\mathbf{u}} - \mathbf{M}_2^T \lambda^{i+1}))\| \\
&\leq \|\frac{\rho}{\tau_2}(\mathbf{u}^{i+1} - \mathbf{u}^i) + \rho \mathbf{M}_2^T (\mathbf{M}_1 \mathbf{w}^{i+1} + \mathbf{M}_2 \mathbf{u}^i + \mathbf{M}_3 \mathbf{k}^i \\
&\quad + \mathbf{M}_4 \mathbf{v}^i) + \mathbf{M}_2^T (\lambda^{i+1} - \lambda^i)\| \\
&= \|\frac{\rho}{\tau_2}(\mathbf{u}^{i+1} - \mathbf{u}^i) + \rho \mathbf{M}_2^T [\mathbf{M}_2(\mathbf{u}^i - \mathbf{u}^{i+1}) \\
&\quad + \mathbf{M}_3(\mathbf{k}^i - \mathbf{k}^{i+1}) + \mathbf{M}_4(\mathbf{v}^i - \mathbf{v}^{i+1})]\| \\
&\leq \|\frac{\rho}{\tau_2} \mathbf{I} - \rho \mathbf{M}_2^T \mathbf{M}_2\| \|\mathbf{u}^{i+1} - \mathbf{u}^i\| + \rho \|\mathbf{M}_2^T \mathbf{M}_3\| \|\mathbf{k}^{i+1} - \mathbf{k}^i\| \\
&\quad + \rho \|\mathbf{M}_2^T \mathbf{M}_4\| \|\mathbf{v}^{i+1} - \mathbf{v}^i\|, \tag{G.4}
\end{aligned}$$

By (19), there exists $\bar{\mathbf{k}} \in \partial f_3(\mathbf{k}^{i+1})$ such that

$$\begin{aligned}
\mathbf{k}^{i+1} &= P_{X_3}(\mathbf{k}^{i+1} - [\bar{\mathbf{k}} + \frac{\rho}{\tau_3}(\mathbf{k}^{i+1} \\
&\quad - (\mathbf{k}^i - \tau_3 \mathbf{M}_3^T (\mathbf{M}_1 \mathbf{w}^{i+1} + \mathbf{M}_2 \mathbf{u}^{i+1} \\
&\quad + \mathbf{M}_3 \mathbf{k}^i + \mathbf{M}_4 \mathbf{v}^i - \frac{\lambda^i}{\rho})))])]. \tag{G.5}
\end{aligned}$$

Then, similarly, we have

$$\begin{aligned}
& \text{dist}(\mathbf{0}, \mathcal{E}_{\mathbf{k}}(\mathbf{y}^{i+1})) \\
&= \text{dist}(\mathbf{k}^{i+1}, P_{X_3}(\mathbf{k}^{i+1} - (\partial f_3(\mathbf{k}^{i+1}) - \mathbf{M}_3^T \lambda^{i+1}))) \\
&\leq \|P_{X_3}(\mathbf{k}^{i+1} - [\bar{\mathbf{k}} + \frac{\rho}{\tau_3}(\mathbf{k}^{i+1} - (\mathbf{k}^i - \tau_3 \mathbf{M}_3^T (\mathbf{M}_1 \mathbf{w}^{i+1} \\
&\quad + \mathbf{M}_2 \mathbf{u}^{i+1} + \mathbf{M}_3 \mathbf{k}^i + \mathbf{M}_4 \mathbf{v}^i - \frac{\lambda^i}{\rho})))])]) \\
&\quad - P_{X_3}(\mathbf{k}^{i+1} - (\bar{\mathbf{k}} - \mathbf{M}_3^T \lambda^{i+1}))\| \\
&\leq \|\frac{\rho}{\tau_3}(\mathbf{k}^{i+1} - \mathbf{k}^i) + \rho \mathbf{M}_3^T (\mathbf{M}_1 \mathbf{w}^{i+1} + \mathbf{M}_2 \mathbf{u}^{i+1} + \mathbf{M}_3 \mathbf{k}^i \\
&\quad + \mathbf{M}_4 \mathbf{v}^i) + \mathbf{M}_3^T (\lambda^{i+1} - \lambda^i)\| \\
&= \|\frac{\rho}{\tau_3}(\mathbf{k}^{i+1} - \mathbf{k}^i) + \rho \mathbf{M}_3^T [\mathbf{M}_3(\mathbf{k}^i - \mathbf{k}^{i+1}) \\
&\quad + \mathbf{M}_4(\mathbf{v}^i - \mathbf{v}^{i+1})]\| \\
&\leq \|\frac{\rho}{\tau_3} \mathbf{I} - \rho \mathbf{M}_3^T \mathbf{M}_3\| \|\mathbf{k}^{i+1} - \mathbf{k}^i\| \\
&\quad + \rho \|\mathbf{M}_3^T \mathbf{M}_4\| \|\mathbf{v}^{i+1} - \mathbf{v}^i\|. \tag{G.6}
\end{aligned}$$

By (21), there exists $\bar{\mathbf{v}} \in \partial f_4(\mathbf{v}^{i+1})$ such that

$$\begin{aligned}
\mathbf{v}^{i+1} &= P_{X_4}(\mathbf{v}^{i+1} - [\bar{\mathbf{v}} + \frac{\rho}{\tau_4}(\mathbf{v}^{i+1} \\
&\quad - (\mathbf{v}^i - \tau_4 \mathbf{M}_4^T (\mathbf{M}_1 \mathbf{w}^{i+1} + \mathbf{M}_2 \mathbf{u}^{i+1} \\
&\quad + \mathbf{M}_3 \mathbf{k}^{i+1} + \mathbf{M}_4 \mathbf{v}^i - \frac{\lambda^i}{\rho})))])]. \tag{G.7}
\end{aligned}$$

Then, like (G.2), we have

$$\begin{aligned}
& \text{dist}(\mathbf{0}, \mathcal{E}_{\mathbf{v}}(\mathbf{y}^{i+1})) \\
&= \text{dist}(\mathbf{v}^{i+1}, P_{X_4}(\mathbf{v}^{i+1} - (\partial f_4(\mathbf{v}^{i+1}) - \mathbf{M}_4^T \lambda^{i+1}))) \\
&\leq \|P_{X_4}(\mathbf{v}^{i+1} - [\bar{\mathbf{v}} + \frac{\rho}{\tau_4}(\mathbf{v}^{i+1} - (\mathbf{v}^i - \tau_4 \mathbf{M}_4^T (\mathbf{M}_1 \mathbf{w}^{i+1} \\
&\quad + \mathbf{M}_2 \mathbf{u}^{i+1} + \mathbf{M}_3 \mathbf{k}^{i+1} + \mathbf{M}_4 \mathbf{v}^i - \frac{\lambda^i}{\rho})))])]) \\
&\quad - P_{X_4}(\mathbf{v}^{i+1} - (\bar{\mathbf{v}} - \mathbf{M}_4^T \lambda^{i+1}))\| \\
&\leq \|\frac{\rho}{\tau_4}(\mathbf{v}^{i+1} - \mathbf{v}^i) + \rho \mathbf{M}_4^T (\mathbf{M}_1 \mathbf{w}^{i+1} + \mathbf{M}_2 \mathbf{u}^{i+1} + \mathbf{M}_3 \mathbf{k}^{i+1} \\
&\quad + \mathbf{M}_4 \mathbf{v}^i) + \mathbf{M}_4^T (\lambda^{i+1} - \lambda^i)\| \\
&= \|\frac{\rho}{\tau_4}(\mathbf{v}^{i+1} - \mathbf{v}^i) + \rho \mathbf{M}_4^T [\mathbf{M}_4(\mathbf{v}^i - \mathbf{v}^{i+1})]\| \\
&\leq \|\frac{\rho}{\tau_4} \mathbf{I} - \rho \mathbf{M}_4^T \mathbf{M}_4\| \|\mathbf{v}^{i+1} - \mathbf{v}^i\|. \tag{G.8}
\end{aligned}$$

It is obvious that

$$\begin{aligned}\|\mathcal{E}_\lambda(\mathbf{y}^{i+1})\| &= \|\mathbf{M}_1\mathbf{w}^{i+1} + \mathbf{M}_2\mathbf{u}^{i+1} + \mathbf{M}_3\mathbf{k}^{i+1} + \mathbf{M}_4\mathbf{v}^{i+1}\| \\ &= \frac{1}{\rho}\|\lambda^{i+1} - \lambda^i\|. \end{aligned}\quad (\text{G.9})$$

By (G.2), (G.4), (G.6), (G.8) and (G.9), we have

$$\begin{aligned}\text{dist}^2(\mathbf{0}, \mathcal{E}(\mathbf{y}^{i+1})) &= \text{dist}^2(\mathbf{0}, \mathcal{E}_\mathbf{w}(\mathbf{y}^{i+1})) + \text{dist}^2(\mathbf{0}, \mathcal{E}_\mathbf{u}(\mathbf{y}^{i+1})) \\ &\quad + \text{dist}^2(\mathbf{0}, \mathcal{E}_\mathbf{k}(\mathbf{y}^{i+1})) + \text{dist}^2(\mathbf{0}, \mathcal{E}_\mathbf{v}(\mathbf{y}^{i+1})) \\ &\quad + \text{dist}^2(\mathbf{0}, \mathcal{E}_\lambda(\mathbf{y}^{i+1})) \\ &\leq 2\left\|\frac{\rho}{\tau_1}\mathbf{I} - \rho\mathbf{M}_1^T\mathbf{M}_1\right\|^2\|\mathbf{w}^{i+1} - \mathbf{w}^i\|^2 \\ &\quad + (2\rho^2\|\mathbf{M}_1^T\mathbf{M}_2\|^2 + \left\|\frac{\rho}{\tau_2}\mathbf{I} - \rho\mathbf{M}_2^T\mathbf{M}_2\right\|^2)\|\mathbf{u}^{i+1} - \mathbf{u}^i\|^2 \\ &\quad + (2\rho^2\|\mathbf{M}_1^T\mathbf{M}_3\|^2 + 2\rho^2\|\mathbf{M}_2^T\mathbf{M}_3\|^2 \\ &\quad \quad + \left\|\frac{\rho}{\tau_3}\mathbf{I} - \rho\mathbf{M}_3^T\mathbf{M}_3\right\|^2)\|\mathbf{k}^{i+1} - \mathbf{k}^i\|^2 \\ &\quad + (2\rho^2\|\mathbf{M}_1^T\mathbf{M}_4\|^2 + 2\rho^2\|\mathbf{M}_2^T\mathbf{M}_4\|^2 + 2\|\mathbf{M}_3^T\mathbf{M}_4\|^2 \\ &\quad \quad + \left\|\frac{\rho}{\tau_4}\mathbf{I} - \rho\mathbf{M}_4^T\mathbf{M}_4\right\|^2)\|\mathbf{v}^{i+1} - \mathbf{v}^i\|^2 \\ &\quad + \frac{1}{\rho^2}\|\lambda^{i+1} - \lambda^i\|^2. \end{aligned}\quad (\text{G.10})$$

Then it is easy to see that Lemma 11 holds for some $\eta > 0$. \square